Length scale correlations of cellular microstructures in directionally solidified binary system

by

Yunxue Shen

A thesis submitted to the graduate faculty
in partial fulfillment of the requirements for the degree of
MASTER OF SCIENCE

Major: Metallurgy

Program of Study Committee:
Rohit Trivedi, Major Professor
Ralph E. Napolitanb
Dennise Vigil

Iowa State University
Ames, Iowa
2002

Graduate College

Iowa State University

This is to certify that the Master's thesis of

Yunxue Shen

has met the thesis requirements of Iowa State University

_____

Major Professor

_____

For the major Program

_____

For the Graduate College

TABLE OF CONTENTS

ABSTRACT

In a cellular array, a range of primary spacing is found to be stable under given growth conditions. Since a strong coupling of solute field exists between the neighboring cells, primary spacing variation should also influence other microstructure features such as cell shape and cell length. The existence of multiple solutions is examined in this study both theoretically as well as experimentally.

A theoretical model is developed that identifies and relates four important microstructural lengths, which are found to be primary spacing, tip radius, cell width and cell length. This general microstructural relationship is shown to be valid for different cells in an array as well as for other cellular patterns obtained under different growth conditions. The unique feature of the model is that the microstructure correlation does not depend on composition or growth conditions since these variables scale microstructural lengths to satisfy the relationship obtained in this study. Detailed directional solidification experimental studies have been carried out in the succinonitrile-salol system to characterize and measure these four length scales. Besides the validation of the model, experimental results showed additional scaling laws to be present. In the regime where only a cellular structure is formed, the shape of the cell, the cell tip radius and the length of the cell are all found to scale individually with the local primary spacing.

The presence of multiple solutions of primary spacing is also shown to influence the cell-dendrite transition that is controlled not only by the processing variables (growth velocity, thermal gradient and composition) but also by the local cell spacing. The cell-dendrite transition was found not to be sharp, but occurred over a range of processing conditions. Two critical conditions have been identified such that only cells are present below lower critics condition, and only dendrites are formed above the upper critics condition. Between these two limits, both cells and dendrites have been found to coexist. In this mixed regime, a critical local spacing is found above which a cell is unstable and forms a dendrite. An analytical expression is developed that relates the critical spacing for the cell-dendrite transition with processing conditions.

1. INTRODUCTION

During the directional solidification of alloys, the solid-liquid interface can assume a planar, cellular or dendritic shape depending on experimental variables, such as the alloy composition (C_0), the growth velocity (V) and the temperature gradient (G) in the liquid at the interface [1-3]. For fixed values of C_0 and G, a planar interface is observed at low velocity. As the externally imposed velocity is increased, a planar interface becomes unstable and forms shallow cells, deep cells and then dendritic structures, as shown in Fig. 1. These different non-planar interfaces cause microsegregation patterns that control many mechanical properties of the material. Microsegregation patterns are governed by the primary or secondary arm spacing and the length of the mushy zone, i.e. the amplitude of cells or dendrites. Consequently, many theoretical and experimental studies (1-6) have been focused on the correlation between the primary spacing and the imposed solidification conditions, i.e. C_0, G and V, which we shall refer to as the control parameters since they are externally imposed upon the system.

There are three critical aspects of cellular patterns that are not yet understood. (1) Theoretical models are based on the solution of mass and heat transport equation with interface energy effect being considered in the boundary condition. This is a free boundary problem in which the shape of the interface is not known a priori, but is determined from the solution that give steady-state growth. The solution of the transport equations gives infinite number of solutions, whereas experimental results show that only a narrow band of solu
tions is selected. The basic criterion, and associated physics, for the selection of cellular pattern have not yet developed. (2) It is now well established that a narrow band of primary spacing is present in a system under given values of the controlled parameters [4-6]. However, for cellular growth in which significant interactions between the neighboring cells occur, the multiple solutions of spacing should also be coupled with the corresponding changes in other microstructural features such as the shape of the cellular front, cell tip radius and the amplitude of the cell.

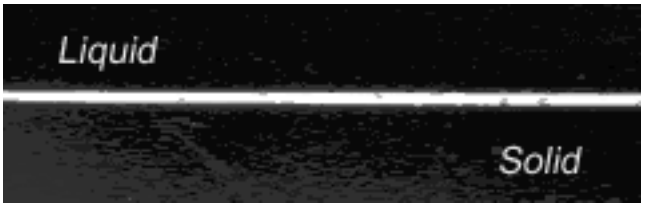

(a)

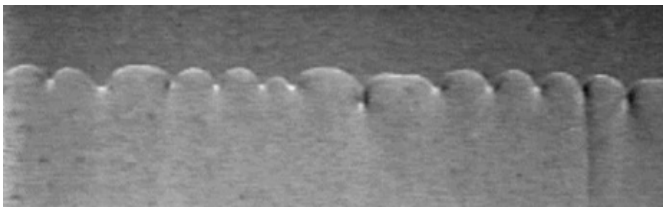

(b)

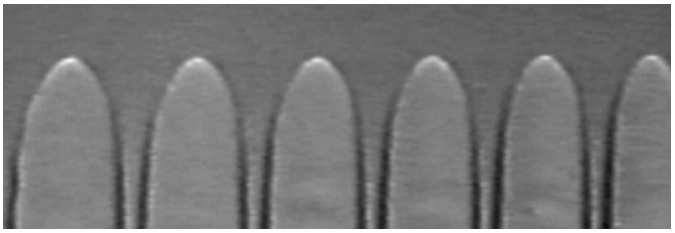

(c)

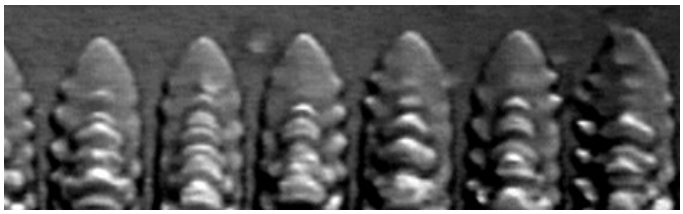

(d)

Fig. 1-1 Interface morphology in SCN-0.7 wt % Salol at G=3.8K/mm
(a) V=0.35μm/s, planar; (b) V=3μm/s, shallow cells;
(c) V=8μm/s, deep cells and (d) V=25μm/s, dendrites.

Since the microstructure evolves in response to the imposed values of control parameters, and there are multiple solutions for a given set of control parameters, there should be a relationship among these micro-structural variables that has not yet been addressed. (3) The condition for the cell-dendrite transition has not yet been established. In this thesis, we shall examine the last two aspects of cellular/dendritic patterns.

For dendritic growth, rigorous mathematical modeling [7] and careful experimental studies [8] have shown that the shape of the interface near the tip deviates negligibly from a parabola. Since the interaction of the solute fields between the neighboring dendrites is small, one can examine the dendrite tip characteristics from the solution of an isolated dendrite. Furthermore, the criterion for the selection of unique dendrite tip radius under given growth conditions has been investigated through rigorous theoretical models that predict that the selection of tip radius is governed by the anisotropy in interface properties [7]. In contrast, the solute field interaction between neighboring cells is significant so that the spacing between cells influences the shape of the interface [9]. In fact, the shape of the tip region varies from nearly planar to parabolic as the velocity is increased from the critical velocity of planar front instability to cell-dendrite transition velocity. The free boundary problem for the solution of cellular growth is thus complex and requires a numerical solution. Several approximate analytical models have been developed under the assumption of some specific interface shape near the tip of the cell that include hemispherical [9, 10], halt elliptical [11] and parabolic [12] shapes of the cell tip region. These assumed shapes do not rigorously give steady-state solution of a cellular array. The determination of the cellular shape is critical since the shape of the interface in intimately connected to the spacing. Also, both the spacing and the shape of the interface dictate the lateral rejection of the solute, which controls the length of the mushy zone and the resulting microsegregation patters in the solid. Consequently, the shape of the cell plays a crucial role in characterizing primary spacing and the length of the mushy zone, and thus the microsegregation pattern so that a more accurate description of the shape is required.

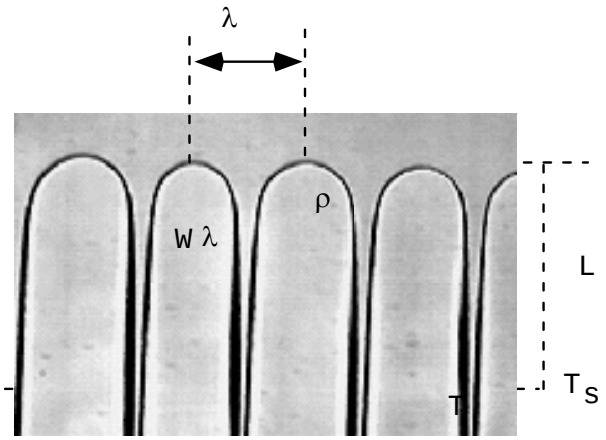

Fig. 1-2. Microstructural length scales: primary spacing (λ), tip radius (ρ), length of the cell above the solid's temperature (L) and the shape parameter (W)

The main focus of this study is to carry out critical experiments that would quantitatively examine the multiple solutions of microstructural variables that exist under given growth conditions. These microstructural variables will be characterized by primary spacing (λ), tip radius (ρ), cell amplitude or the length of the mushy zone above the solid's isotherm (L) and a dimensionless shape parameter(W). To be more precise, we shall examine how a fixed set of input parameters (G, V and C_0) gives rise to a multiple sets of output parameters, which are shown in Fig. 2, and to determine if any correlation exists among these four microstructure parameters. We shall show that these multiple sets of the output parameters are not independent, and a relationship exists among them. An analytical expression will be developed to quantify this correlation among all microstructural variables.

We shall also examine how the presence of a spectrum of primary spacing influences the cell-dendrite transition. We shall show that this transition not only depends on the values of control parameters, but it is also influenced by the local spacing since the transition initiates at a location where the local spacing is the largest in a given array. Consequently, there is a growth regime in which both cells and dendrites grow simultaneously in an array [8,13].

In order to determine the shapes precisely, experiments were carried out in a model transparent system of succinonitrile-salol whose properties are listed in Table 1. The dynamics of pattern formation in this system was recorded on a video and the video pictures were digitized to determine the shape of the interface near the tip region. We shall first describe the experimental technique, and then present the results of experiments in the following form: (i) A presence of a spectrum of spacing for fixed values of control parameters. These results will be obtained over a range of V, G, and C_0, which include both cellular and dendritic patterns. (ii) Shape of the interface near the tip region for cells and/or dendrites in the same array and in arrays obtained under different growth conditions. The shape of the interface, up to about twice the primary spacing distance, will be characterized by two parameters (ρ and W). (iii) The effect of local spacing on cell-dendrite transition will then be quantitatively investigated to include the critical condition that takes into account both the processing parameters and the local spacing. These experimental results will then be analyzed quantitatively to establish the physics that governs the correlation between cell spacing, cell shape and the length of the mushy zone.

2. EXPERIMENTAL PROCEDURE

2.1 Directional Solidification Apparatus

The directional solidification equipment used in this study is similar in principle to that described by Jackson and Hunt [26]. Fig. 2-1. is a schematic drawing of the experimental arrangement for in-situ observation of solidification microstructures. Several modifications were made to achieve higher accuracy and precision required for the present experimental study, which as described by Mason and Eshelman [27].

The solidification experiment was carried out by moving a sample in a thermal gradient field. This thermal gradient is built by holding hot and cold chambers at a fixed distance apart with a machined lexan block. To obtain a stable thermal gradient, a lexan block is placed below the sample and between the hot and cold chambers to reduce the thermal convection due to air flowing below the sample. The sample covered with a piece of thin glass slip was moving between hot and cold chambers in order to reduce air convection from the top. Two oil bathes (Neslab Instrument, Inc.) were used to control the temperature of hot and cold chambers within ± 0.01°C and to maintain a stable temperature gradient. The temperature gradient at the interface was obtained from a thermal profile measured by a thermocouple that was placed inside the cell. Fig. 2-2. Shows the results of the measurement of temperature gradient for two typical conditions. The magnification was about 50 x when the experimental photo file was opened by Photoshop software.

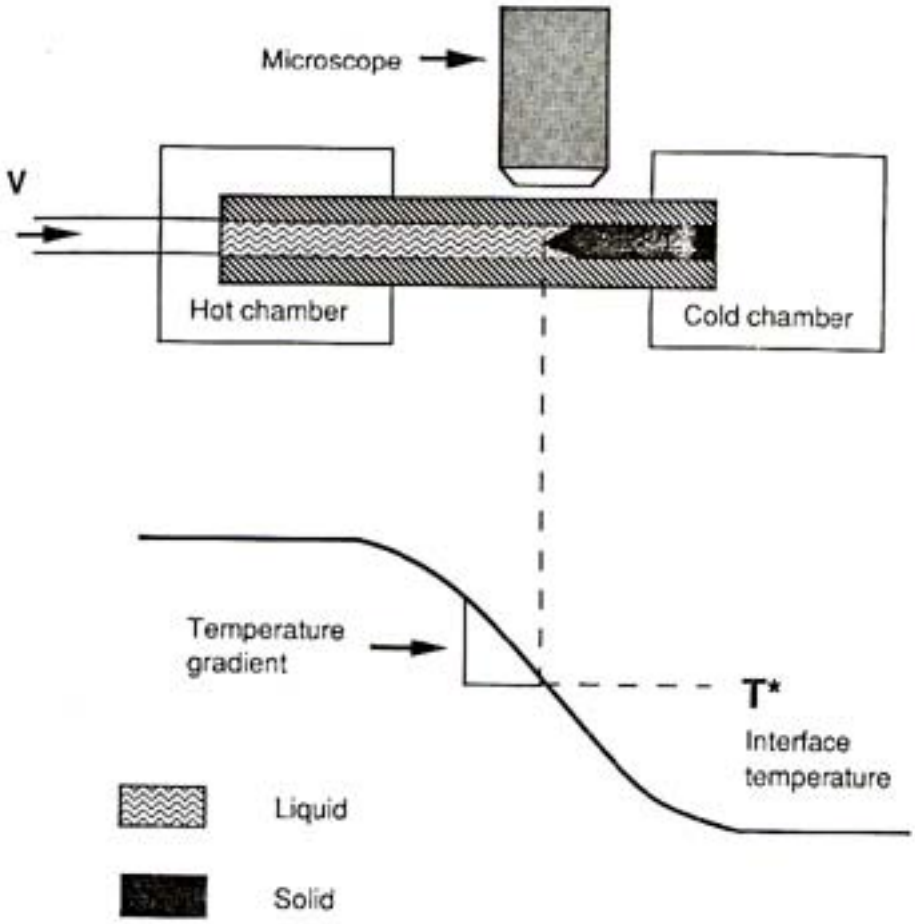

Fig. 2-1. A Schematic drawing of the directional solidification experimental arrangement for in-situ observation of interface shape.

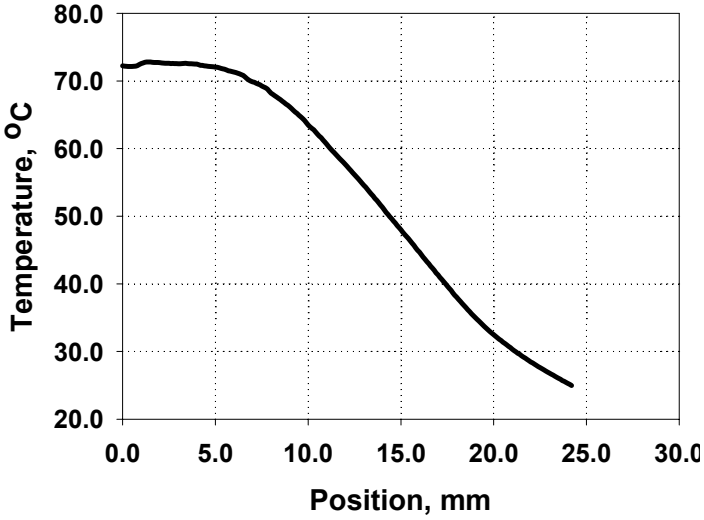
80.0
70.0
60.0
50.0
40.0
30.0
20.0
Temperature, °C
0.0
5.0
10.0
15.0
20.0
25.0
30.0
Position, mm

(a)

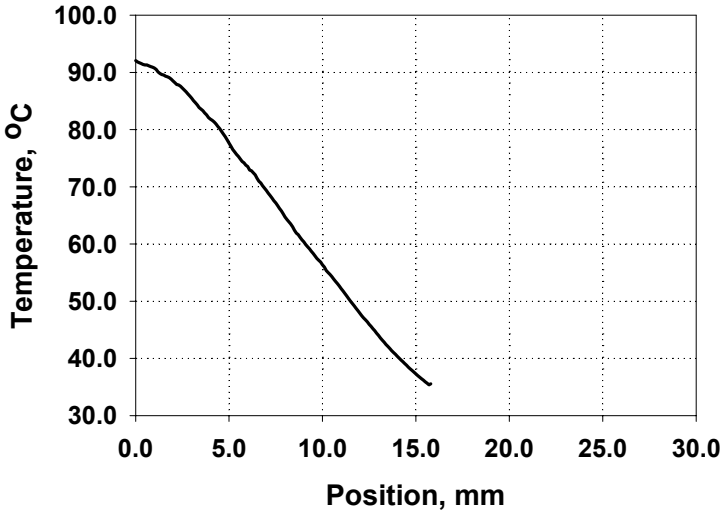
100.0
90.0
80.0
70.0
60.0
50.0
40.0
30.0
Temperature, °C
0.0
5.0
10.0
15.0
20.0
25.0
30.0
Position, mm

(b)

Fig. 2-2. The measurements of thermal profile: (a) low G case and (b) high case.

2.2 Alloy Preparation

The succinonitrile-salol (the chemical formula for succinonitrile is $NCCH_2CH_2CN$ and for salol is 2-$(HO)C_6H_4CO_2C_6H_5$) organic alloy system was studied since it is optically transparent, which allows in-situ observations of interface pattern dynamics. It has a low thermal entropy of melting, and has a body centered cubic crystal structure, so that its solidification characteristics are similar to most metallic systems. The principal properties and the phase diagram of succinonitrile -salol system, shown in Fig.2-3, have been characterized by Kirkaldy, et al [15, 16]. The binary alloy has a low melt temperature which

Table 1. Material and Alloy Property Parameters in Succinonitrile-salol System

	Succinonitrile [1]
Melting point	331.24 K
Entropy of fusion	11.21 J/mol K
Density of solid	1.016×10^3 Kg/m^3
Density of liquid	0.907×10^3 Kg/m^3
Thermal conductivity of solid	0.224 J/ms K
Thermal conductivity of liquid	0.223 J/ms K
Solid-liquid interface energy	8.95×10^{-3} J/m^2
Gibb-Thompson Coefficient	0.64×10^{-7} K m

Molecular weight	80.09 g/mol
Succinonitrile-salol [2]	
Diffusion coefficient in the liquid (D)	$0.8 \times 10^{-9} m^2/s$
Liquidus slope (m)	-0.68 K/ wt %
Equilibrium partition coefficient (k)	0.16
Molecular weight of salol	214.22 g/mol

[1] Parameters of succinonitrile from M. A. Eshelman, Ph. D. Thesis (Iowa State Univ.) 1987.

[2] Parameters of succinonitrile-salol from L. X. liu and J. S. Kirkaldy, Scripta Metallurgica et Materialia 29 (1993)801.

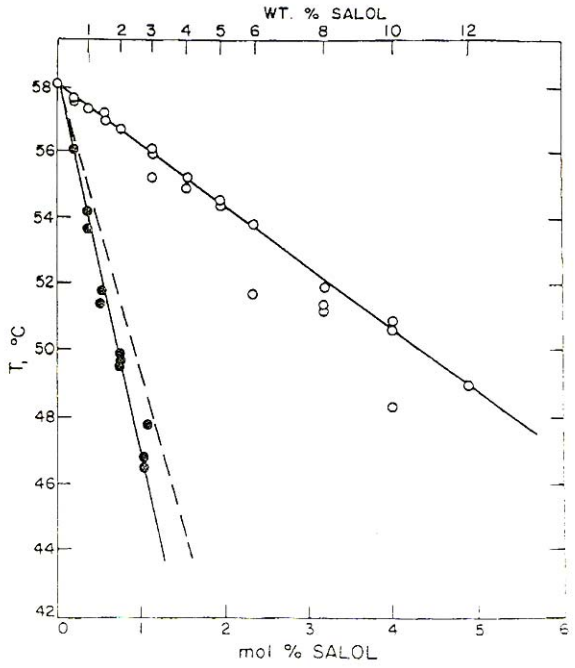

Fig. 2-3. Succinonitrile-rich side of the phase diagram in SCN-salol system. Solid lines are best-fit lines for experimental points. The broken line shows calculated results [35]

is convenient for the filling of the alloy into the experimental cell and for controlling the cooling and heating devices of the directional solidification apparatus. The relevant material properties of succinonitrile and succinonitrile-salol are listed in table 1.

Experiments were carried out with salol composition varying from 0.7 wt % to 2wt %. As received succinonitrile was first distilled and zone refined. Original as-received succinonitrile of 99 % purity was distilled at 75-90 ˚C in a standard distillation apparatus [22]. The distilled SCN was collected into a 1200 mm long tube under vacuum condition and sealed and then zone refined. A known quantity of salol was added and the alloy was melted and filled into a Hele-Shaw cell under an inert atmosphere of dry nitrogen.

2.3 Sample Cell Dimensions and Filling Procedure

Two different sample cells made of glass, with a rectangular cross section in this study. The dimensions of the sample cells were 200mm x 4mm x 200μm and 200mm x 2mm x 100μm. Generally three identical sample cells were placed on the translation stage of the directional solidification apparatus in a given experiment. One of these three cells contained a thin calibrated thermocouple inside and the cell was filled with pure succinonitrile. The other two samples were filled with the succinonitrile-salol binary alloy. The final accurate composition of the alloy was further established by comparing the planar solid/liquid interface positions at steady-state between cell with pure succinonitrile and cells filled with succinonitrile –0.7wt % salol. For each growth condition, the cell with thermocouple was placed to characterize the thermal profile. The results in the two other samples were used to check the reproducibility of the results.

The sample thickness was ≤ 200μm, so that the convection effects were negligible. To prevent absorption of the moisture in the air, the process of filling the sample cell was carried out under an inert nitrogen atmosphere.

2.4 Experimental Procedure

In the experiment, a single crystal seed was made before solidification to eliminate the grain boundary effect, which may influence primary spacing distribution. Before each solidification run, the cell, except the single seed crystal, was first held in the temperature gradient grade higher than the melt temperature for at least 10 hours to ensure thermal equilibrium.

For the sample with SCN-0.7 wt % salol, the temperature gradient was keep constant and the velocity was the only variable used to cause changes in the interface morphology. The change in interface shape, for steady state growth, was obtained for each velocity. In order to check the change in shape during the cell-dendritic transition, the velocity was increased in steps, and at each velocity the sample was solidified for a sufficient time to reach its new steady state. The experimental conditions for each composition are summarized in Table 2.

Table 2. Summary of experimental conditions for Succinonitrile-salol sample

Sample composition (wt %)	**Temperature gradient (K/mm)**	**Velocity (μm/s)**
0.7	2.6	1, 3, 5, 7, 9, 11, 13, 15.
	3.8	4, 5, 8, 11, 15, 20, 25
	5.0	9, 10, 11, 14, 18, 20, 22,25
1.0	3.8	4, 5, 6, 6.5, 7, 7.5, 8, 8.5, 9
1.5	3.5	0.625, 1.0, 1.25, 1.875, 2.5

2.0	3.8	0.5, 0.625, 1.0, 1.25, 2.5

2.5 Procedure for Characterizing Tip Radius, Cell Shape and Cell Spacing

During observation, the interface patterns were video imaged and the video pictures were digitized and used for quantitative analysis. The analog information of the video picture was digitized by the computer software Snap.

Five different steps were used to obtain digital information of cellular shapes:

a. Display the digital picture in the Photoshop software and find the exact magnification (M) by comparing the photo to a standard scale.

b. Record the shape position original data (X, Y)

c. Change position data (X, Y) to (x, y). The (x, y) is with micrometer unit and cellular tip as the origin $x=(X-X_{tip})/M$; $y=(Y_{tip}-Y)/M$,

d. Take one half of the cell with corresponds the spacing λ, and reflect this shape. Get the dimensionless cellular shape plot (r, z). Here $r=y/\lambda$ and $z=x/\lambda$, λ is the local cellular spacing and $-0.5<r<0.5$.

e. Regression dimensionless cellular shape (r, z) by a function z(r), $z = -ar^2(1 + br^2 + cr^4 + dr^6)$, $-0.5<r<0.5$. The property of z(r) is that it is dimensionless (independent of units)

An example of the digital information of cellular shape: at G=3.8K/mm, V=4μm/s, for the cell with primary spacing λ=142μm, is given in Fig.2-4, where the equation was obtained as $z = -0.72r^2(1 + 12r^2 - 88r^4 + 1348r^6)$

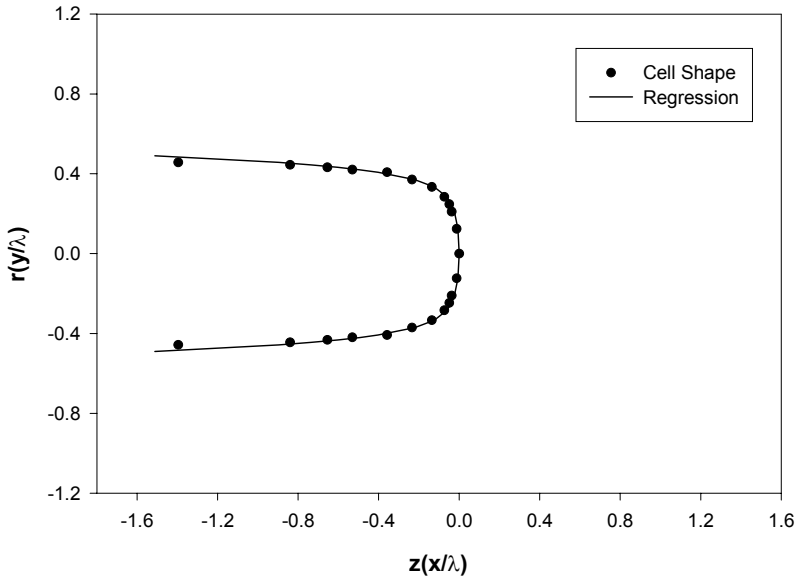

Fig.2-4 Example of a digitized cellular shape with a curve-fitting expression.

3. EXPERIMENTAL RESULTS

3.1 Spectrum of Spacing

Experimental results showed the presence of three distinct regimes of microstructures. (1) At low velocities, only cells were present, (2) cells and dendrites coexisted at intermediate velocities, and (3) only dendrites were present at higher velocities. In all the three regimes, a spectrum of spacing was observed. Fig. 3-1a shows a cellular array and the distance between neighboring cells were measured and the distribution of local spacing in this array is shown in 3-1b. A dendritic array and the spacing distribution in the array are shown in Fig. 3-2. The minimum and the maximum spacing in an array were measured for different cellular and dendritic arrays obtained under different growth

conditions and a plot of $\lambda_{max}/\lambda_{min}$ versus V/V_c for different G is shown in Fig. 3-3 for o.7 wt % salol. In the regime where both cells and dendrites were present, only the distance between two neighboring cells and neighboring dendrites were measured. Note that this ratio for cell increases initially from 1.2 to 1.4 and then decreases when both cells and dendrites are present in an array. For dendrites, the ratio increases with velocity when both cells and dendrites are present, but approaches a constant value of 1.52 when only dendritic array is present. Note that the maximum spacing is not twice the minimum spacing. The presence of a distribution of spacing in an array is crucial since it also gives rise to distribution in other microstructural features, and influences the cell dendrite transition.

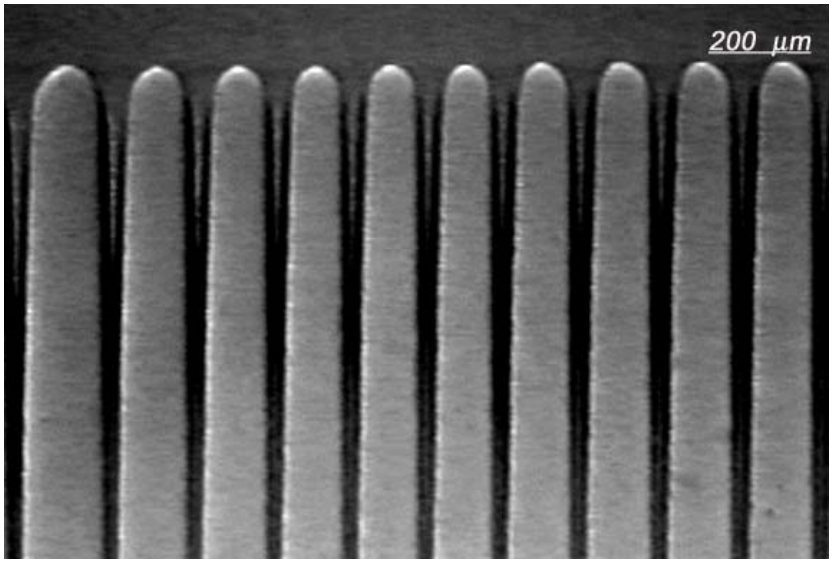

(a)

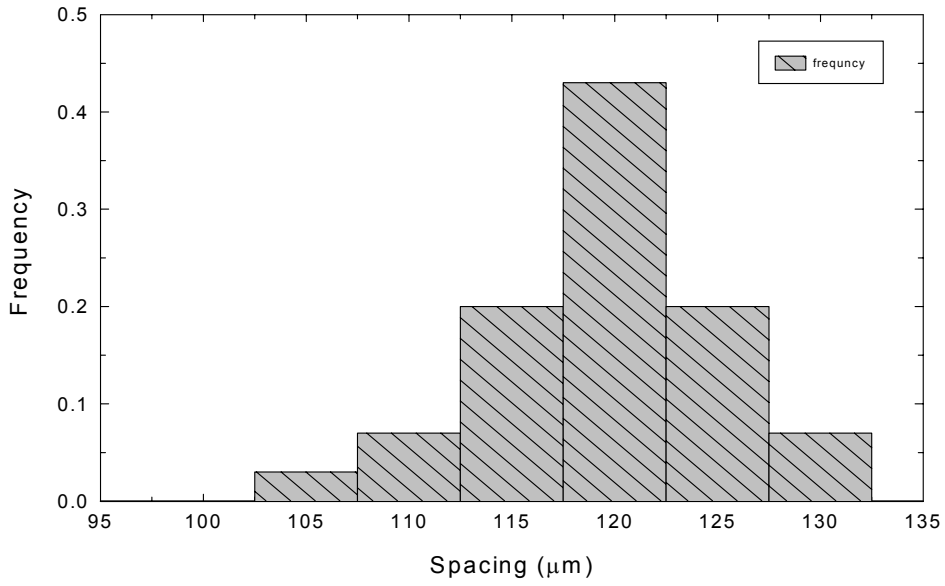

(b)

Fig.3-1. Steady state cellular growth in SCN-0.7 wt % salol, G=3.8 K/mm, V=5 μm/s; (a) Photograph of a cellular, and (b) Cellular spacing distribution.

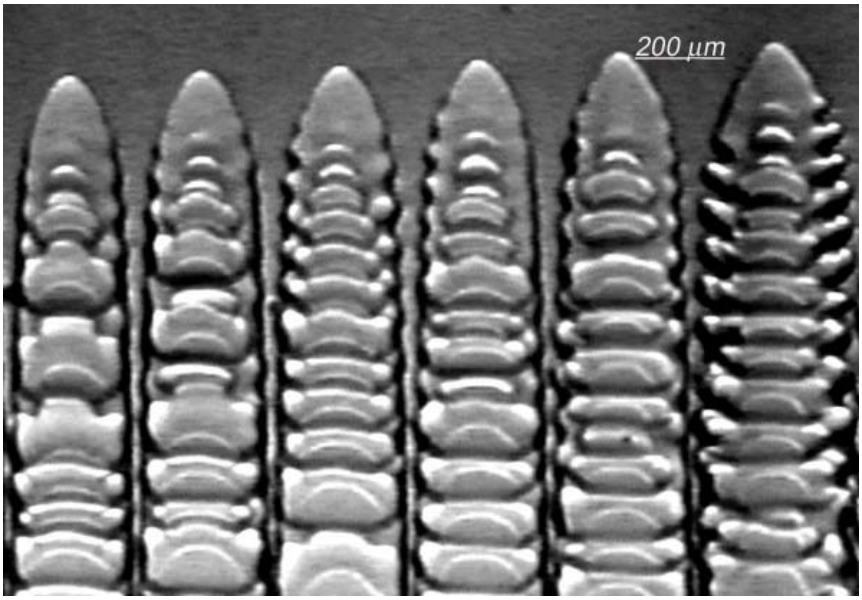

(a)

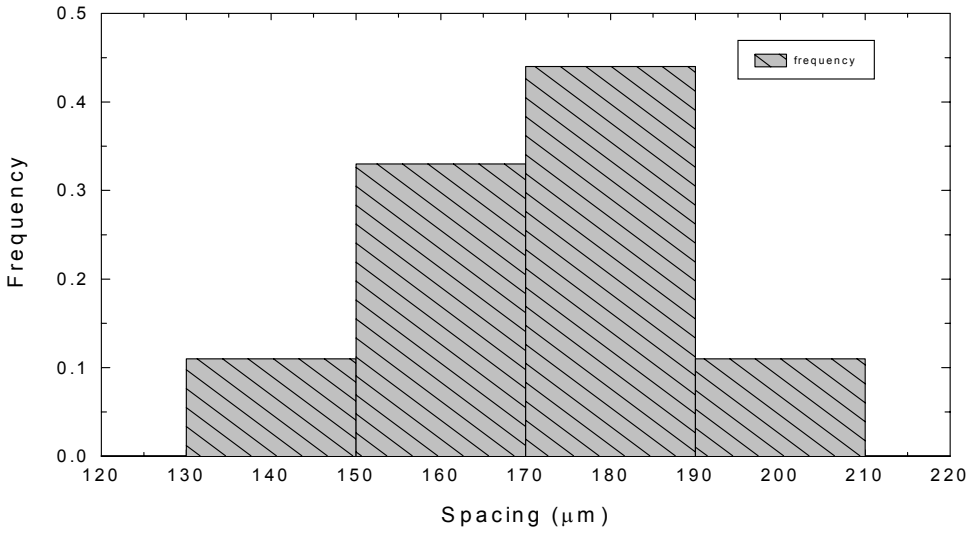

(b)

Fig.3-2. Steady state dendritic growth in SCN-0.7 wt % salol, G=3.8 K/mm, V=20 μm/s. (a) A photograph of a dendritic array, growth and (b) dendrite spacing distribution.

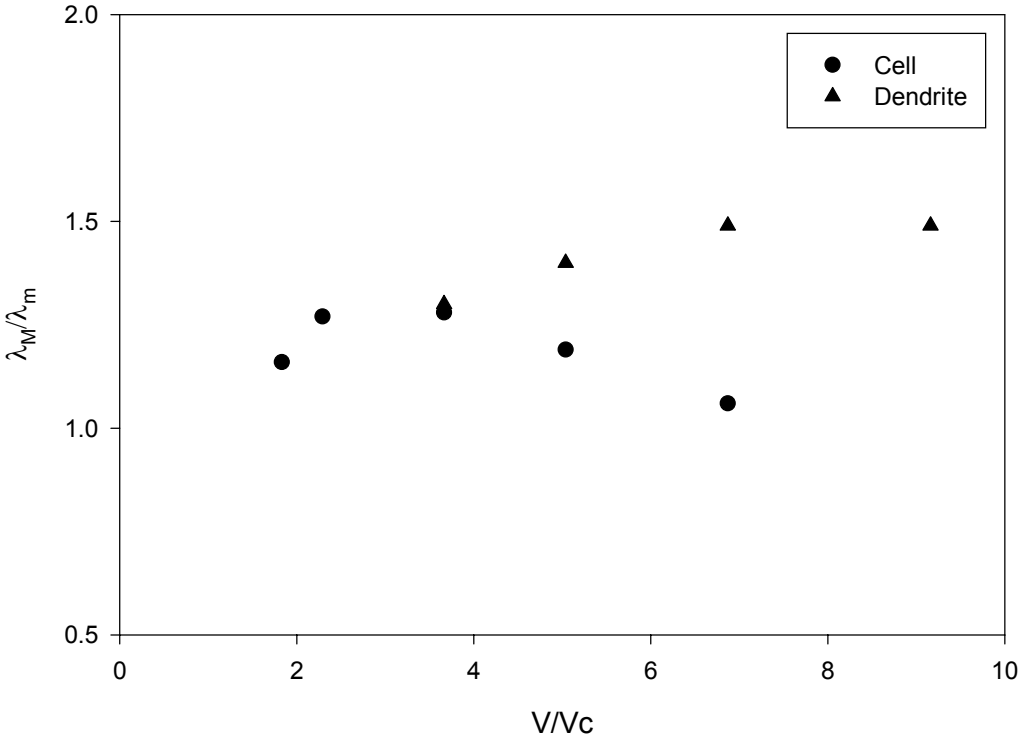

Fig. 3-3. The variation in the ratio of maximum to minimum primary spacing in an array as a function of V/V_c for cellular and dendritic arrays. The growth input parameters: SCN-0.7 wt % salol, G=3.8 K/mm, Vc=2.24 μm/s;

3.2 Shape of the Interface

3.2.1 Mathematical Representation

The shape of the cell is influenced by the value of the local cell spacing. In order to obtain a quantitative description of the cell shape, the cell tip region was fitted to an analytical expression. The primary spacing in this study were of the order of 100 μm and only one row of cellular/dendritic array was observed in all experiments. Since the

thickness of the sample is roughly twice the spacing, the shape of the interface in the tip region will be three-dimensional. However, the cellular interface will touch the glass walls at a distance roughly twice the primary spacing, after which the cell shape will be two-dimensional. Consequently, all the shapes were characterized only up to a distance of one to two λ behind the tip. Since the neighboring spacing are different, only a half cell with corresponding spacing was used to characterize its shape. The shape of the cell, with the origin at the tip of the cell, can be expanded in a power series:

$$-x = \alpha\, y^2 + \beta\, y^4 + \gamma\, y^6 + \eta y^8 + \ldots\ldots \qquad (1)$$

where x is in the growth direction and y is normal to the growth direction. The origin of the coordinate system was at the tip of the cell or dendrite. Higher order terms in y were also considered, but the first four terms were found to describe the shape completely. Note that the coefficient α is related the tip radius as $\alpha=0.5\rho$. The results for two velocities at G=3.8 K/mm and one velocity at G=4.2 K/mm are shown in Table 3, for succinonitrile – 0.7wt % salol. The local spacing in an array varied from 142.1 to 189.5 μm, for V=4.0 μm/s and from 108.8 to 138.6 μm for V = 5.0 μm/s. The shape of the interface and tip radius value were found to vary with the variation in local spacing. Since the local spacing is different as two sides of the cell each half of the cell was considered separately and related to the corresponding to local spacing.

Table 3. Summery of Cellular Shapes at Low Velocities

(Succinonitrile-0.7 wt % salol, G=3.8K/mm)

	λ (μm)	ρ (μm)	λ/ρ	$\beta x10^{-6}(\mu m^{-3})$	$\gamma x10^{-9}(\mu m^{-5})$	$\eta x10^{-13}(\mu m)$	W
V=4.0 μm/s (G=3.8 K/mm)							
	142.1	98.7	1.44	3.0	-1.1	8.3	0.32
	149.1	103.5	1.44	2.6	-0.86	5.9	0.32
	161.4	112.1	1.44	2.1	-0.58	3.4	0.32
	189.5	131.6	1.44	1.3	-0.23	1.1	0.32
V=5.0 μm/s (G=3.8 K/mm)							
	108.8	27.2	4.0	24.8	0	8.9	0.52
	110.5	27.6	4.0	23.7	0	8.0	0.52
	115.8	28.9	4.0	20.6	0	5.7	0.52
	117.5	29.4	4.0	19.7	0	5.2	0.52
	119.3	29.8	4.0	18.8	0	4.7	0.52
	122.8	30.7	4.0	17.3	0	3.8	0.52
	138.6	34.6	4.0	12.0	0	1.6	0.52
V=7.5μm/s (G=4.2 K/mm)							
	109.6	39.1	2.8	11.2	-15.0	70.1	0.53
	119.2	42.6	2.8	9.3	-9.9	39.4	0.53
	126.0	45.0	2.8	7.8	-7.5	26.7	0.53
	137.5	49.1	2.8	6.0	-4.8	14.5	0.53
	145.3	51.9	2.8	5.1	-3.7	9.9	0.53
	149.0	53.2	2.8	4.7	-3.2	8.3	0.53

The data were converted to dimensionless length scales by dividing the distance with the local spacing of the cell: z = x/λ and r = y/ λ. In this dimensionless form the shape of the interface becomes

$$z = -\mathbf{a}r^2\left(1+\mathbf{b}r^2+cr^4+dr^6+.....\right) \qquad (2)$$

The general form can be written as:

$$z(r) = -\frac{\lambda}{2\rho}r^2(1+\sum_{n=1}^{\infty}a_{2n}r^{2n}) \qquad (3)$$

The nondimensional constants a_{2n}, where n from 1 to 4, are related to the dimensional constants α, β, γ and η as: $\mathbf{a} = \alpha\lambda = \lambda/2\rho$, $a_2 = \beta\lambda^3/\alpha$, $a_4 = \gamma\lambda^5/\alpha$ and $a_6 = \eta\lambda^7/\alpha$. The parameter **a** is related to the tip radius and the cell spacing, whereas the parameter $\mathbf{a_{2n}}$ shows the departure of the shape from a parabolic shape.

Since **a** is related to the tip radius, the tip radius was first determined by using nine points in the tip region and calculating the tip radius, ρ, from the relationship: $\rho = [1+x'^2]^{3/2}/x''$, in which x' and x" are the first and second derivatives of y with respect to y. The radius is then related to nondimensional parameter **a** by the relationship: $\mathbf{a} = \lambda/2\rho$.

In order to numerical describe the cell shape, we introduce W, the dimensionless width parameter defined as:

$$W = \frac{1}{\left[1+\sum_{n=1}^{\infty}\frac{2}{n+2}a_{2n}\left(\frac{1}{2}\right)^{2n}\right]^{1/2}} \qquad (4)$$

All $\mathbf{a_{2n}}$ parameters are included in W. W is the relative width of the cell and it represents a deviation from a parabolic shape since it is unity when the entire cell shape is a parabola, and is less than unity when the shape deviates from a parabola. Note that W can be seen as representing the relative width of the cell since W is small when the width is small compared to a parabola with the same tip radius value. The origin of this definition of W will be given in the discussion section. The values of W were determined for different cells in the same array, and also for different growth conditions.

3.2.2 Cells only Regime

The data for V= 5.0 μm/s at G=3.8 K/mm are plotted in Fig. 3-4. The cell tip radius is found to increase as the local spacing increases. However the value of λ/ρ was found to be nearly constant and independent of local spacing. Thus, the value of the parameter **a** is constant for all cells in an array. In order to validate this observation, the shapes of the cells in an array were plotted in dimensionless coordinates. Fig. 3-5 (a) shows three different cells which had different local spacing. However, these three cell shapes were found to superpose not only near the tip region, but also over the distance equal to about twice the primary spacing. Similar superposition of shape has been observations by Akamatsu et al. in the carbon tetrabromide system [14]. Fig. 3-5(b) shows the same result as in Fig. 3-5(a), but with the z-axis scale expanded to show an excellent matching in the tip region. This superposition implies that the value of the constant W will also be the same for all cells in an array and this was indeed observed, as shown in Table 3. Similar results were found for the cellular array grown at V = 4.0 μm/s and at high temperature gradient G=4.2 K/mm, V=7.5 μm/s. The superposition in this growth condition was shown in Fig. 3-6a, and a comparison was given between the dimensionless cell shape and the curve by the regressed power series. Since the cell shape superposes in a given array, the regressed power series bears the same form and the same W and dimensionless tip radius values.

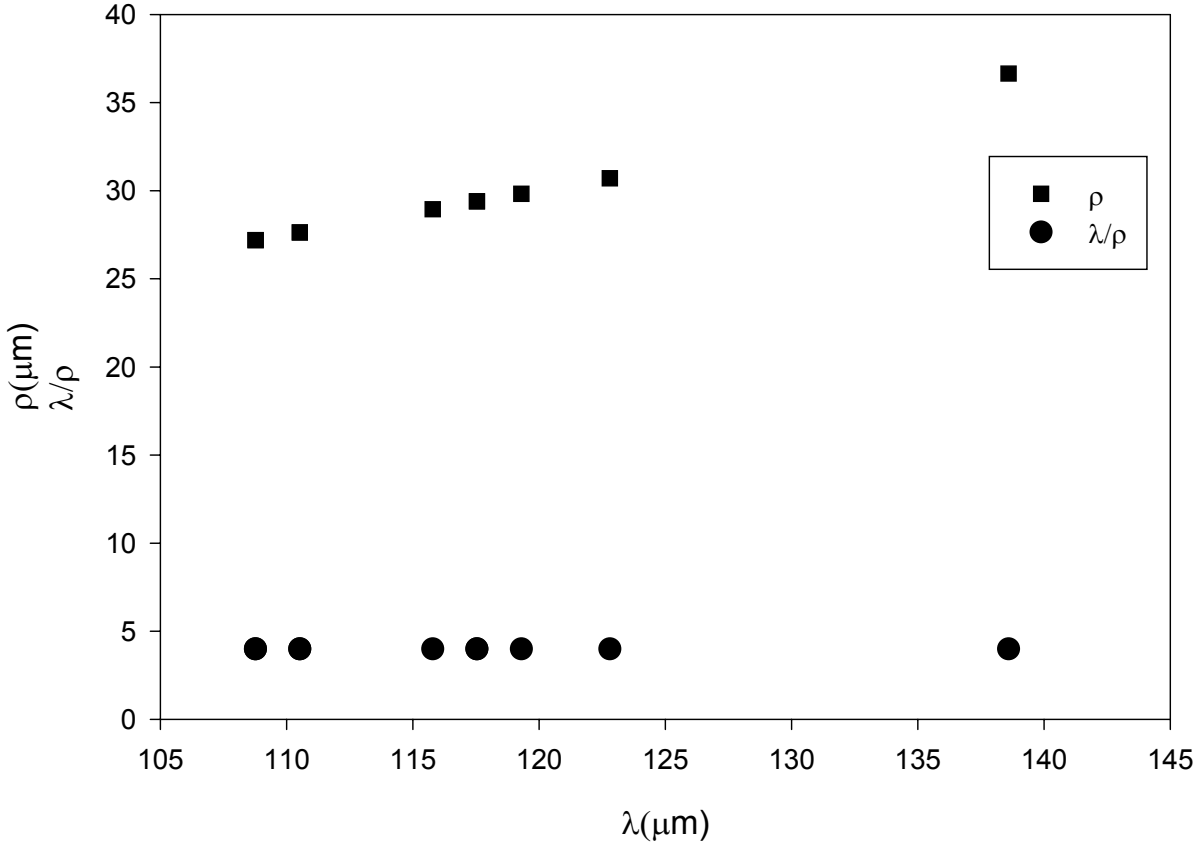

Fig. 3-4. The variation in the tip radius and in the ratio of cellular spacing to tip radius with cellular spacing. V=5.0 μm/s and G=3.8K/mm.

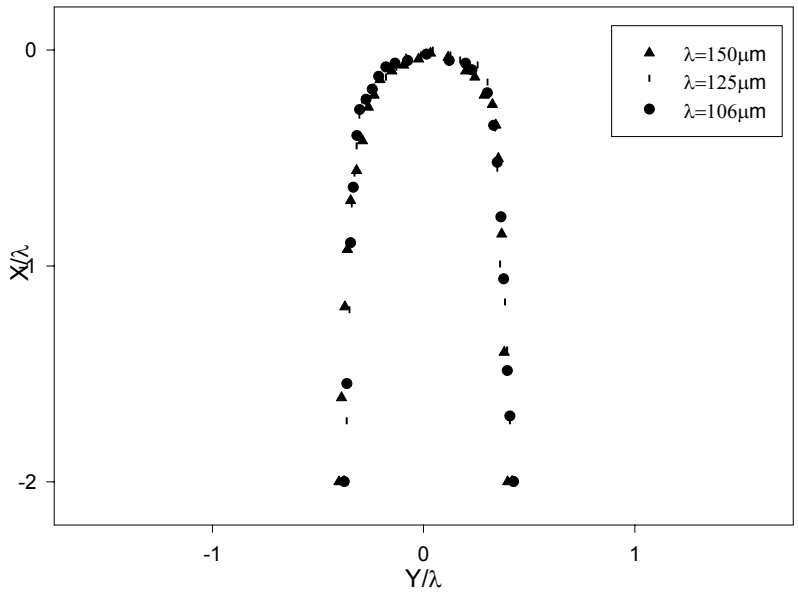

(a)

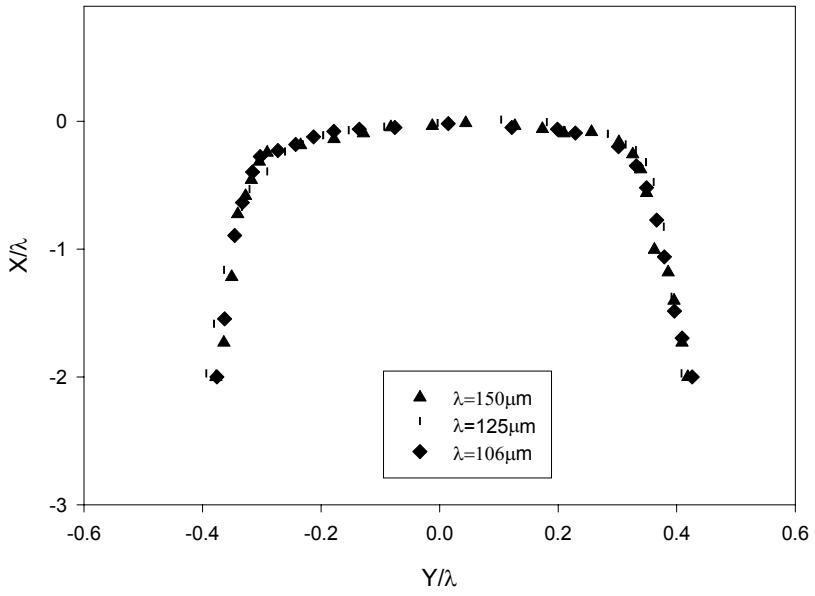

(b)

Fig.3-5. (a) The superposition of the shapes of three cells in an array in dimensionless Coordinates, V=5.0 μm, G=3.8K/mm. The shape is invariant over a significant distance behind the tip. (b) An expanded scale in the y direction for the superposition in shown Fig. (a) to show a good match in the tip region.

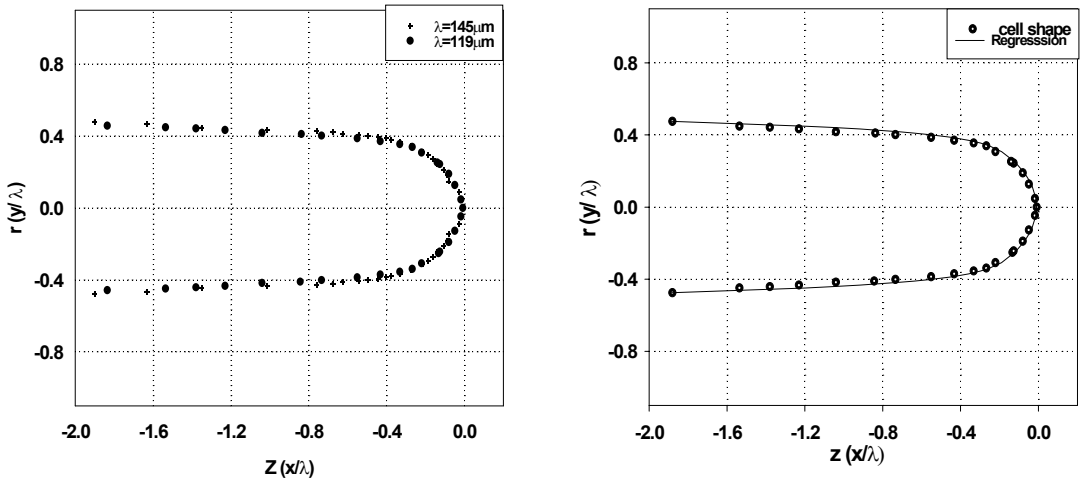

(a) (b)

Fig. 3-6 (a) The shape is invariant over the entire length of the cell. (b) A theoretical expression describing the shape is shown by a solid line.

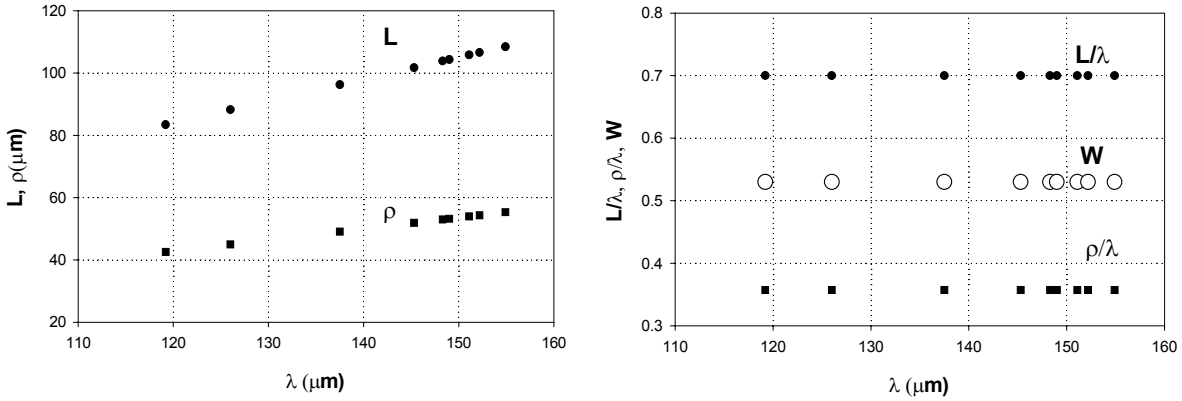

(a) (b)

Fig. 3-7 (a) The variations in the tip radius, ρ, and the length, L, for cells in a given array. (b) The variations in λ/ρ,W. and L/λ for cells in this array. (C_0=0.7 wt % salol, V=7.5 μm/s and G=4.2K/mm)

3.2.3 Cell and dendrite Coexistence

When the velocity was increased above 7.5 μm/s in succinonitrile-0.7 wt % salol, both cells and dendrites co-existed in an array and the superposition of cell shapes of shape was not precisely obeyed. Small differences in values of **a** and **W** were obtained for cells in the same array. The values of **a** and **W** for different velocities are shown in Fig. 3-8. The bars show the range of spacing observed in an array. Note that a significant variation in ρ with λ is present. However the variation in **a** in a given array was small and within the circle shown for the point. The value of **a** increases with velocity since the tip radius decreases faster than the decrease in primary spacing. The value **W** also increases with an increase in V so that the shape of the cell tends towards a parabolic shape (W=1).

3.2.4 Dendritic Regime

In the regime where only dendritic structures were presented, the shape of the tip was found to be parabolic and the value of W=1 was observed for all dendrites.

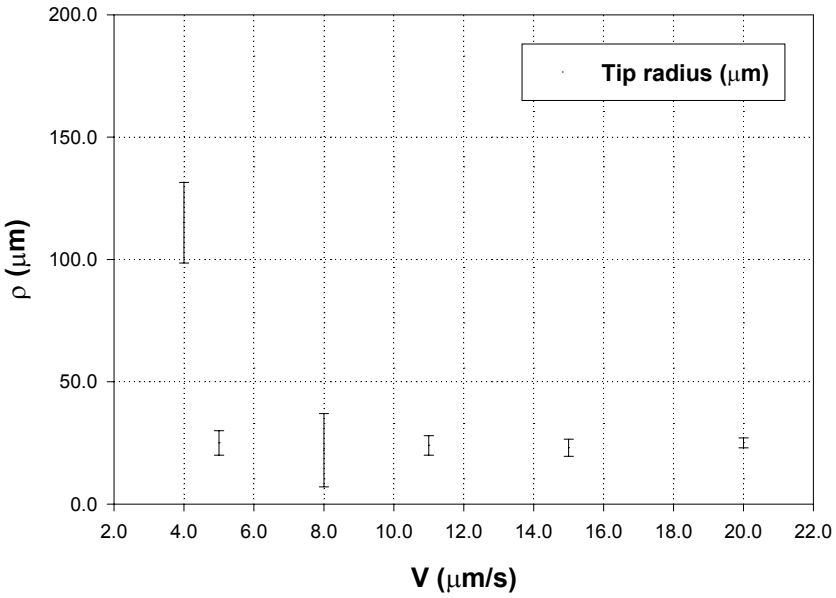

(a)

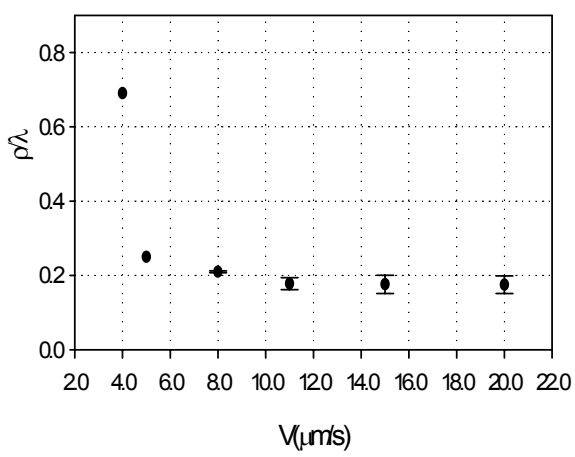

(b)

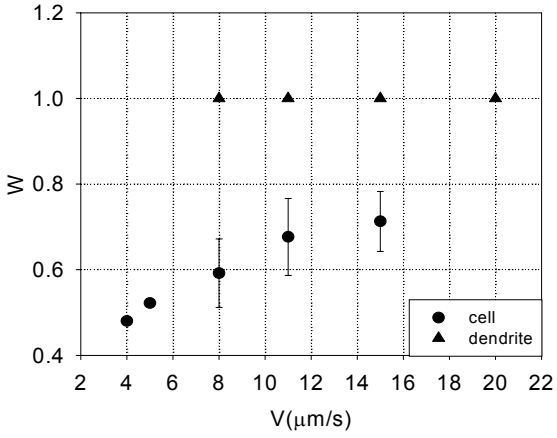

(c)

Fig. 3-8 (a) The variation in (a) tip radius ρ, (b) the ρ/λ and (c) W with growth velocity

3.3 Cell-dendrite Transition

A regime of coexistence of cells and dendrites were observed so that cells and dendrites both form under fixed growth conditions: G, V and C_0. Thus, the transition from cell to dendrite is believed to depend on the local spacing also. Thus detailed experimental studies were carried out to characterize the cell-dendrite transition as a function of velocity and local primary spacing. Figure 3-9. shows the photo of co-existence of cells and dendrites in an array for an experiment at V = 15 μm/s, with G = 3.8 K/mm and C_0 = 0.7 wt % salol. Note that instability for dendrite is examined in the plane of the arrays only. The instability observed on the top is due to the large depth (200μm) of the sample cell. When the velocity was increased, more cells transformed to dendrites and at V = 20 μm/s only dendrites were present. When both cells and dendrites were present, the dendrite spacing was larger than the cell spacing. The range of cells and dendrites at different velocities is shown in Fig. 3-10. In order to qualifiedly establish the effect of local spacing on the cell-dendrite transition, local spacings were measured for steady state growth conditions. In an array, when both cells and dendrites are present, dendrite spacings were found to be larger than cellular spacing, as shown in Fig. 3-10. The spectrums of local spacing at each velocity are also shown. It was observed that a critical cell spacing $\lambda_{c/d}$, exists at a given velocity such that for local spacing larger than the $\lambda_{c/d}$ the cell transforms to a dendrite. This critical spacing was determined by examining the dynamical process and the smallest local spacing of cell was identified when that cell began to transform into a dendrite. If the local spacing was smaller than $\lambda_{c/d}$, cells remained stable. To examine the dynamics of cell-dendrite transition, initial, a cellular array was established and then the velocity was increased slowly until some cells transfer to dendrites. The variation in the shape of the tip region along the cell-dendrite transition is obtained in Fig.3-11.

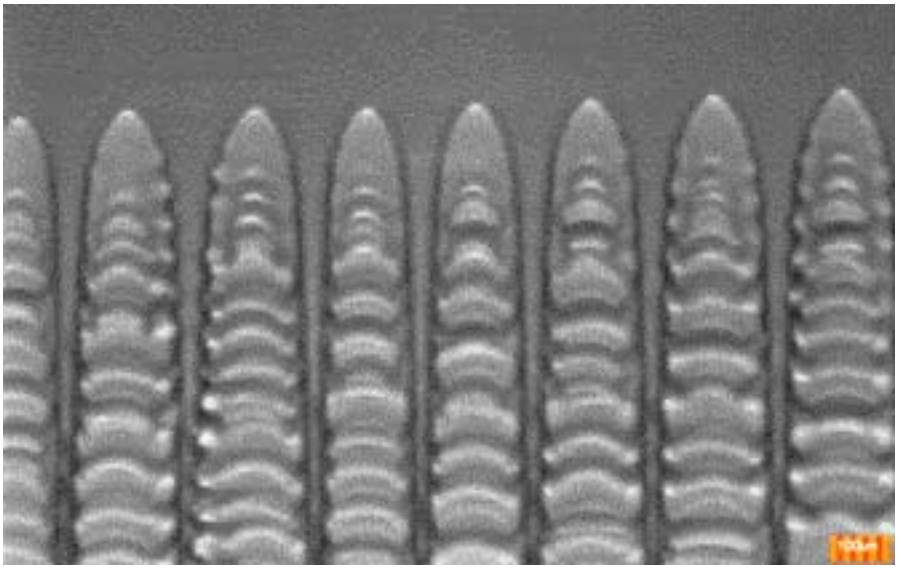

(a)

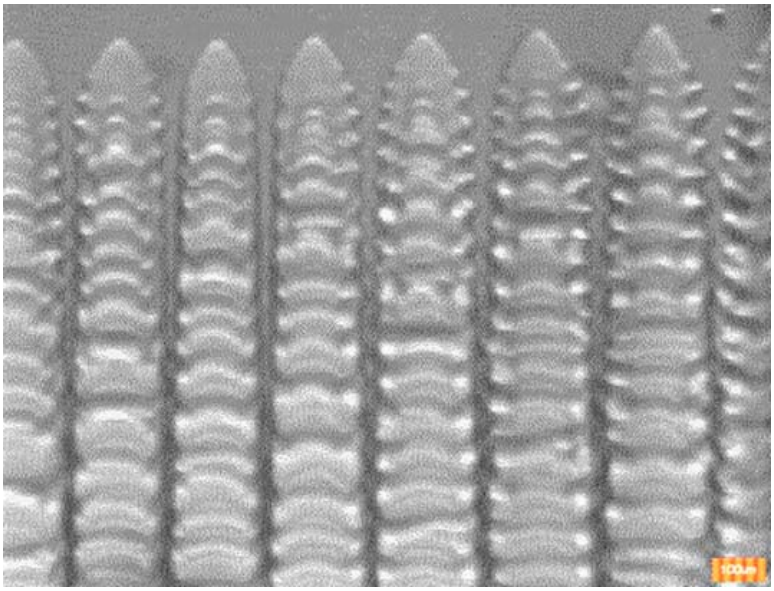

(b)

Fig.3-9. Photographs of coexistence of cell and dendrite in SCN-0.7 wt % salol G=3.8 K/mm. (a) V=15.0μm/s and (b) V=20.0μm/s.

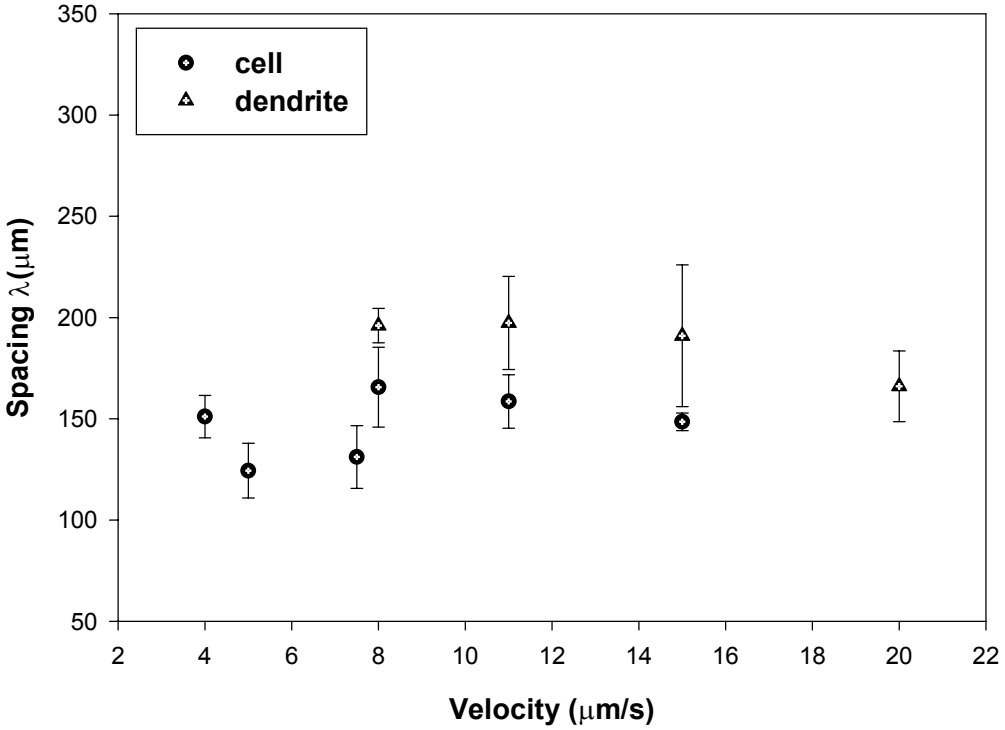

Fig.3-10. The variation in cellular and dendritic spacing as a function of velocity in succinonitrile-0.7 wt % salol directionally solidified. The range of spacing observed in an array at each velocity is shown by the bar on each point.

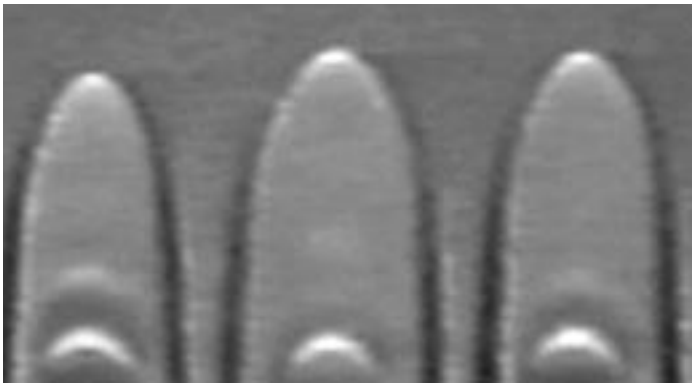

(a)

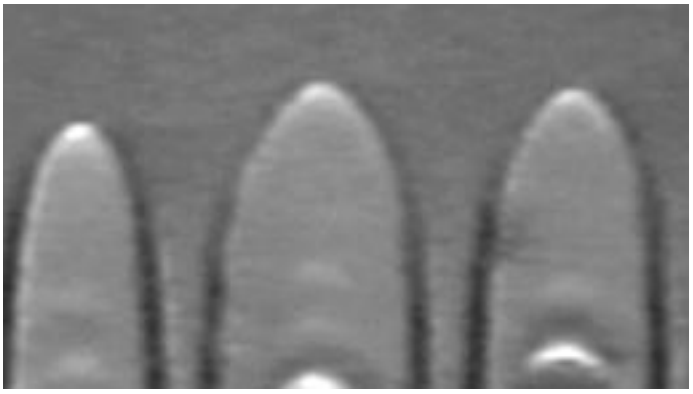

(b)

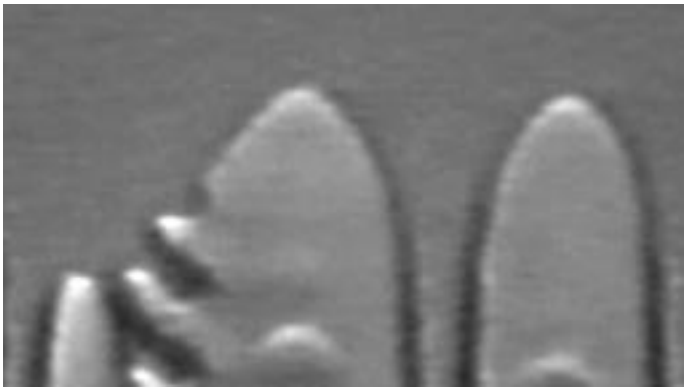

(c)

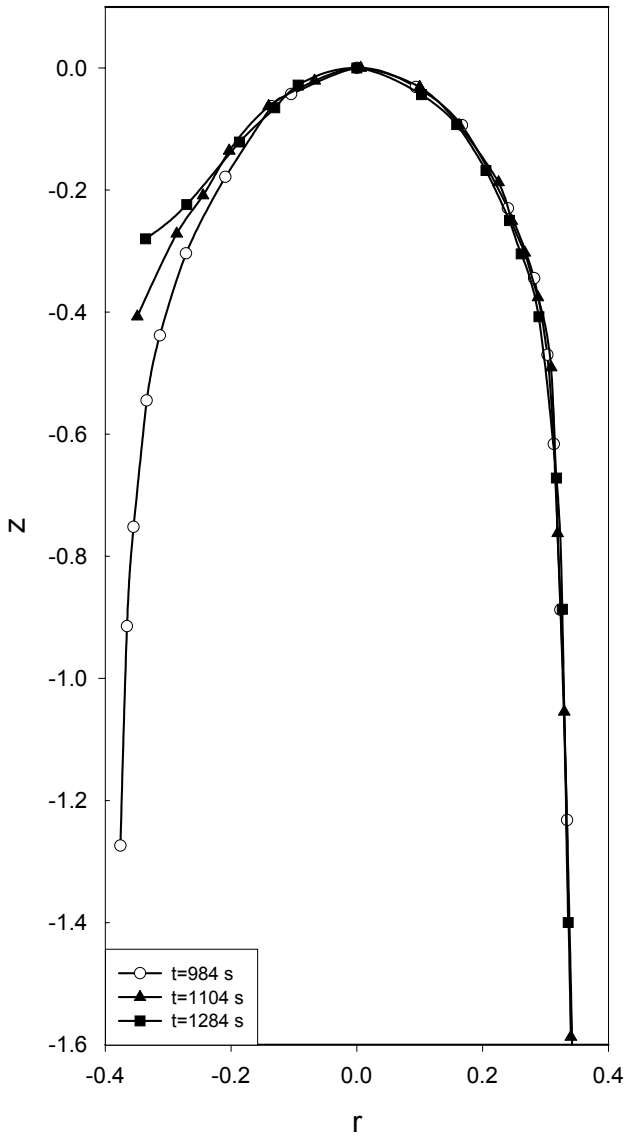

(d)

Fig.3-11. Changes in the shape of the tip region with time as the cell transforms to a dendrite. SCN-0.7 wt % salol, G=3.8K/mm, V=11.0 μm/s. (a) t= 984 s. (b) t=1104 s, (c) 1284 s and (d) comparison of the tip shape for the above three instants. The time was started from the beginning of the experiment. The shape of the tip region can be fitted by analytical functions: right half: a=2.8 and W=0.64 for all figures; left half: a=3.21 for all shapes and W=0.7 for t=984s and W=1 for both t=1104s and 1284s.

The critical low spacing at which a cell transformed to a dendrite was determined as a function of velocity and thermal gradient. The critical spacing, $\lambda_{cd,}$ was found to decrease with an increase in velocity. Experiments were carried out over the entire range of

velocity where both cells and dendrite co-exist for three temperature gradient values in the 0.7 wt % alloy and the results are shown in Fig. 3-12 (a) and (b). The experimental data from the samples with 1.0 wt % and 1.5 wt % salol were shown the similar results of Fig. 3-12.

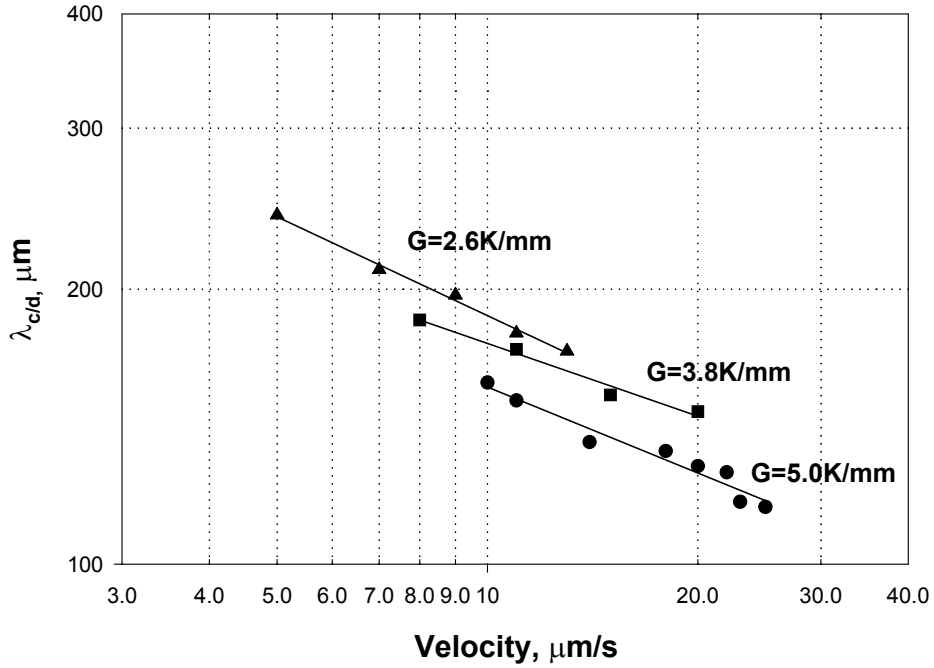

(a)

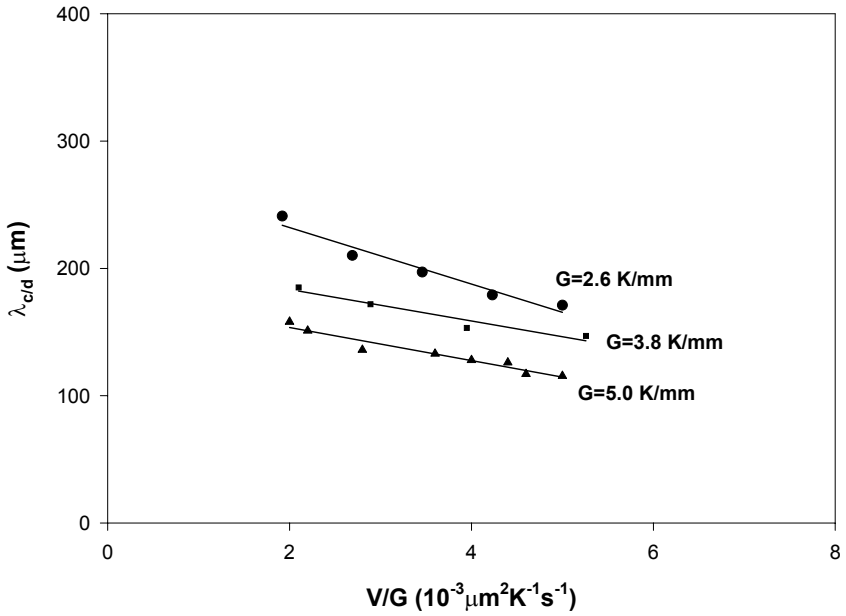

(b)

Fig. 3-12. Experimental data of cellular-dendritic transition spacing in SCN-0.7 wt % salol, system. **.** (a) The transition spacing as a function of (a) velocity and (b) velocity divided by temperature gradient were measured at G=2.6K/mm, G=3.8K/mm and G=5.0K/mm.

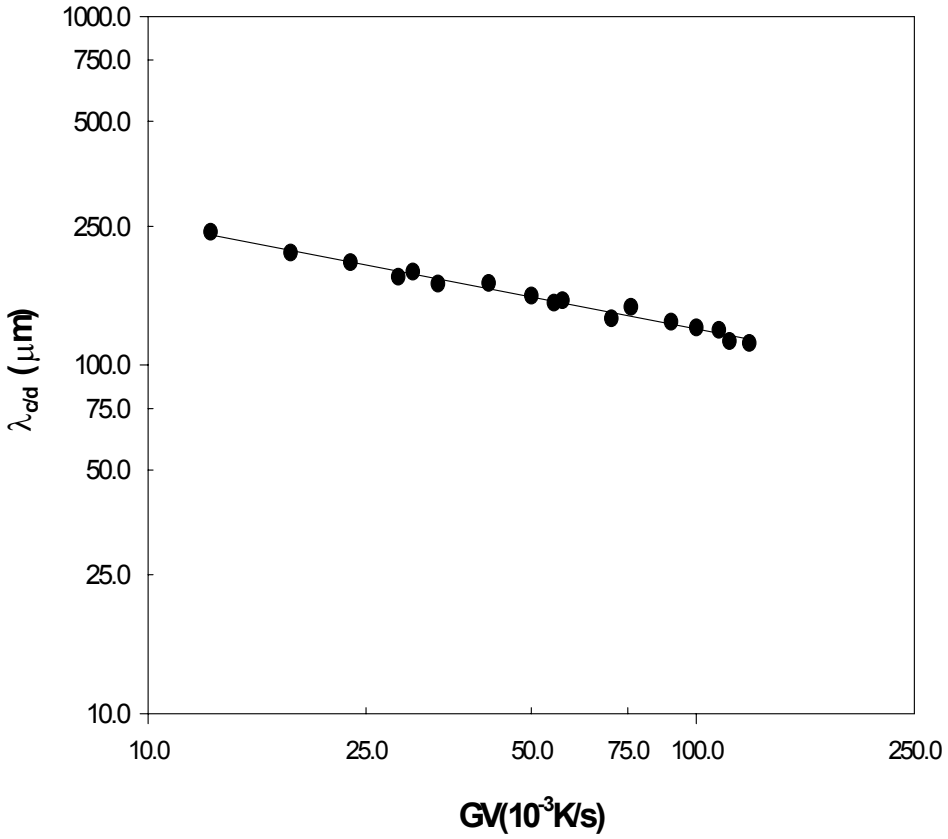

Fig. 3-13 Critical cell/dendrite transition spacing and transition condition for different composition

4. DISCUSSION

The discussion section will be divided as followed: we first develop an expression that correlates different microstructural scales in a cellular array. Next we shall examine the range of spacing that is observed in a given array, and show how the presence of a range of spacing influences cell-dendrite transition.

4.1 Microstructural Scales Correlation

Experimental results have shown that for a given set of control parameters, a range of primary spacing is present in an array. We have shown that this variation in primary spacing is also accompanied by corresponding variations in the tip radius and the shape of the cell. It is reasonable to assume that a certain relationship exists among these microstructure variables for a given value of the control parameters. We shall now develop this relationship by considering a global mass balance in the liquid in the half-cell region, as described by Han and Trivedi [4]. During steady state growth, the value of the integral over a closed path in the liquid mast be zero. One can transform the volume integral to a surface integral and require that the net flux in the closed region must vanish under steady state growth conditions. Using this procedure, the following relationship was obtained by Han and Trivedi [4]:

$$\int_0^{\lambda/2} y x(y)\, dy = -\frac{\lambda^2 L}{8} \qquad (5)$$

where L is proportional to the length of the mushy zone, and is given by

$$L = (T_t - T_s)/G \qquad (6)$$

in which T_t and T_s are the cell tip and solidus temperature of the alloy. L is the length of the cell from the tip to the solidus isotherm, as shown in Fig.1-2. The tip temperature will be a function of local spacing, and it will increase as the spacing increases. Thus, L will increase with spacing. We can now rewrite this relationship in terms of dimensionless parameters, and substitute the expression of the shape function obtained in this study. By writing the left hand side of equation (5) in terms of dimensionless coordinates, (z,r),

$$z(r) = -\frac{\lambda}{2\rho} r^2 (1 + \sum_{n=1}^{\infty} a_{2n} r^{2n})$$

and integrating, we obtain

$$16\, L' \rho' = 1 + \sum_{n=1}^{\infty} \frac{2}{n+2} a_{2n} \left(\frac{1}{2}\right)^{2n} \qquad (7)$$

where L'= L/λ, and ρ` =ρ/λ

$$16\, L' \rho' = 1 + \sum_{n=1}^{\infty} \frac{2}{n+2} a_{2n} \left(\frac{1}{2}\right)^{2n} \qquad (8)$$

The above equation gives an important correlation between the microstructural scales, and can be written as

$$4\, W (\rho' L')^{1/2} = 1 \qquad (9)$$

in which W is the dimensionless width parameter defined as

$$W = \frac{1}{\left[1 + \sum_{n=1}^{\infty} \frac{2}{n+2} a_{2n} \left(\frac{1}{2}\right)^{2n}\right]^{1/2}} \qquad (10)$$

W is the measure of the width of the cell and it represents a deviation from a parabolic shape since it is unity when the entire cell shape is a parabola, and is less than unity when the shape deviates from a parabola. Note that W can be seen as representing the width of

the cell since W is small when the width is small compared to a parabola with the same tip radius value. The microstructural length scale relationship can now be written as

$$[\frac{\rho}{\lambda}\frac{L}{\lambda}]^{1/2} 4W = 1 \qquad (11)$$

Equation (11) is the key result which shows that for a given set of input parameters (G, V and C_0), we obtain output (or microstructural) parameters, (W, ρ, λ and L) that are related by a unique relationship for steady state cellular growth.

We shall now examine the interactions among different microstructural length scales that are present in equation (11). These microstructural features evolve when the interface becomes nonplanar. When the interface is planar, solute transport is one-dimensional. However, as the planar interface becomes unstable, some solute is rejected laterally. The magnitudes of the microstructural scales thus depend upon the extent of the lateral rejection of solute. Just above the critical velocity for planar front stability, a majority of solute is rejected ahead of the interface and only a small amount of solute is rejected laterally in the intercellular region. This small amount of lateral rejection of solute is accomplished by having a large tip radius, small amplitude and smaller W or greater deviation from a parabolic shape with the same tip radius. As the velocity is increased, more solute is rejected laterally, which requires sharpening of the tip radius. Also, a greater amount of solute is rejected in the intercellular region that leads to larger amplitude and a larger W. At some higher velocity, W approaches unity and the shape of the interface become parabolic. At this point sidebranches appear and cells transform to dendrites.

One of the key aspects of our result is that equation (11) predicts a unique relationship among microstructural variables only, i.e. it does not contain composition or processing parameters, it is thus valid for all steady state cellular structures obtained under different input parameters and in different binary alloy systems. Note that each of these microstructural parameters will be a function of input parameters (G, V, C_0) and phase

diagram characteristics. Detailed theoretical models still need to be developed to precisely correlate each individual microstructural scale with input parameters.

4.2 Relationship with Cell Amplitude

Three distinct regimes of microstructures were observed. For SCN-0.7wt %salol:

(i) At V≤ 8.0 μm/s, only cells were observed in an array.

(ii) A coexistence of cells and dendrites in an array was observed over a range of velocities, 8.0 < V < 20.0 μm/s. As the velocity was increased in this transition zone, more cells transformed to dendrites.

(iii) At V ≥ 20.0 μm/s only dendrites were present, at temperature gradient G=3.8K/mm.

Since the local primary spacing varies, the cell tip radius and the cell shape are influenced by the local spacing. Due to the difference in primary spacing on the two sides of a given cell, each cell is not exactly symmetrical. Thus, each half of the cell (from the tip to the base) was first considered and a mirror image was imposed to obtain a symmetrical shape.

For succinonitrile – 0.7 wt % salol, at G=3.8 K/mm, only cells were observed at V = 4.0, 5.0 and 7.5 μm/s. In this cell only regime, both ρ and L were found to increase as the local spacing increased, as shown in Fig. 3-7, as the values of in λ/ρ and L/λ were found to be constant and independent of the local spacing for a given growth velocity, as shown in Fig. 3-7. Also the value of W was found to be constant for all cells in any array. For succinonitrile-0.7 wt % salol, we obtained the data of L, ρ and λ and listed in Table 4.
Using the results for V = 5.0 μm/s λ/ρ=4 and λ/L=1.08, we obtain W = 0.52. The shape of a cell in the array for V=5.0 μm/s, after non-dimensionalization by the local spacing, was fitted by a power series of the form

$$Z(r) = -2r^2 * \left(1 + 16r^2 + 80r^6\right) \qquad (13)$$

Table 4. Quantitative comparison of the predicted W with experimentally determined value from the power series expansion of observed cells in an array					
Velocity, $\mu m\ s^{-1}$	ρ/λ	L/λ	W(eq. 7)	Power series of a cell in the array	W(eq. 5)
V=5.0	0.25	0.93	0.52	$Z(r) = -2r^2 * \left(1 + 16r^2 + 80r^6\right)$	0.5
V=7.5	0.36	1.45	0.53	$Z(r) = -1.4r^2 * \left(1 + 11.2r^2 - 170r^4 + 963r^6\right)$	0.53

4.3Primary Spacing Distribution

Our results have characterized the spectrum of primary spacing that is present in an array, and we obtained $\lambda_{max}/\lambda_{min}$ to vary from 1.3 for low velocity cells to 1.5 for dendrites. This spectrum occurs due to the multiple solutions of λ. The limiting values of the spectrum are governed by the stability of cells in an array. When $\lambda < \lambda_{min}$, the cell becomes narrower with sharper tip radius, and gets eliminated, whereas when $\lambda > \lambda_{max}$, the tip radius becomes large, and the tip becomes unstable and splits. In the theoretical models [5, 6] it has been assumed that the maximum spacing would be twice the minimum spacing since above this spacing tip splitting will occur and two stable cells of minimum spacing will form. We have observed that this is not true. The maximum spacing varies from 1.3-1.5 times the minimum spacing. This is due to the sidewise migration of neighboring cells once a new cell forms by tip splitting. A similar conclusion has been reached for dendritic growth by Han and Trivedi [4] in the succinonitrile-acetone system and by Tewari et al. in the Al- Cu system [18], who obtained the ratio of about 1.4 -1.45. Han and Trivedi clearly showed that a dendrite initiates from a ternary branch when the

local spacing is only 1.4 times the final spacing, and as the tertiary arm becomes a dendrite, the neighboring dendrites move laterally to increase the spacing.

The ration of the maximum to the minimum spacing for cell goes through a maximum. In the regime where both cells and dendrites coexist, the ratio decreases as the fraction of cells in an array decreases. Near the upper transition condition, only a few pairs of cells were present. Theoretical models have examined the minimum stable spacing only, and assumed that the maximum spacing will be about twice the minimum spacing [5,6]. Our experimental results show a more complex relationship and detailed theoretical model need to be developed to understand the physics behind it.

4.4 **C**ell-dendrite Transition

4.4.1 **C**ell-dendrite Transition under Constant Composition

For the sample with the composition of SCN 0.7 wt % salol, when the growth velocity was increased to 8.0μm/s where both cells and dendrites were present, the above superposition of shape in dimensionless condition was not obeyed. The values of λ both for cells and dendrites at different velocities are shown in Fig. 3-10 in which the bars show the narrow spacing range of values observed in an array. For cells, according the calculation based on cellular shapes from experiments, the value of W increased with an increase in V, shown in Table 2, so that the shape of the cell tended towards a parabolic shape. When only dendrites were present, W was found to be equal to 1 for all dendrites. Formation of sidebranches causes a discontinuous change from W=0.71 to W=1, was shown in Fig.3-8, the dendritic transition of the left half of the cell. This result shows that the change to a parabolic tip is accompanied by the formation of sidebranches so that the cell-dendrite transition criterions based on a parabolic tip shape and on the formation of sidebranches are identical.

We have characterized the transition from cells to dendrite when sidebranches form, and shown that this transition must take into account the local primary spacing. In essence, the transition conditions should be controlled by V, G, C_0 and $\lambda_{c/d}$. In fact, this transition is not unique, but occurs locally so that for a given G and C_0, a range of velocity-spacing combination is present over which both cells and dendrites coexist.

The regime in witch both cells and dendrites coexist was identified by determining the transition velocity as a function of thermal gradient and local spacing. However, when plotted against V/G, Fig.3-12, the two limiting values of the parameter V/G were found that were independent of thermal gradient, as shown in Fig. 3-12. When the minimum spacing at witch cells become dendrite was plotted as a function of the dimensionless parameter V/G, it was found that only cells exist when $V/G < (V/G)_{min}$, and dendrite exist when $V/G > (V/V_c)_{max}$. The minimum and the maximum values of the ratio were found to be 3.2 and 6.7 respectively, for the alloy composition of SCN-0.7 wt % salol.

The value of the critical cellular spacing, $\lambda_{c/d}$, at witch a cell transition to a dendrite was, however, found to depend upon the thermal gradient as shown in Fig.3-12. Thus, the dendrite will form if the spacing is larger than the above critical spacing, whereas cell will be stable if it is less than the critical spacing.

The maximum stable cell spacing should be close to the minimum dendrite spacing in the region where both cells and dendrite coexist. Thus one would expect that the critical spacing for the transition will be close to the minimum stable dendrite spacing in an array. However, the cell spacing at witch the cells become unstable and form dendrites is slightly higher than the maximum stable cell spacing. Furthermore, once a cell becomes a dendrite, the dendrite will migrate laterally since the dendrite spacing will be higher that the initial cell spacing. Consequently, in the cell-dendrite coexistence range, the transition spacing will correspond to the spacing that lies between the maximum stable cell spacing and the minimum stable dendrite spacing. This relationship was obtained as $\lambda_{c/d}(GV)^{1/3} = 60\ \mu m K^{-1/3} s^{-1/3}$, which relationship is different from the minimum stable dendrite

spacing relationship obtained by Hunt and Lu [5], especially in the value of the exponent of G. Note that if the primary spacing were kept constant, then the critical velocity of transition increases as the gradient decrease. On the other hand, if the thermal gradient is kept constant, then the critical velocity increases as the spacing is decreased at higher velocity.

4.4.2 Composition Effect in **C**ell-dendrite Transition

From the discussion in 4.4.1, the cell-dendrite transition velocity range may shift at different thermal degree, but the range of V/G almost constant at different G. So the study of composition effect on the cell-dendrite transition can be focused on the transition vs. V/G. Several samples with composition of SCN- 0.7, 1.0, 1.5 and 2 wt % salol were prepared for this study and the transition range of V/G vs. composition were plotted in Fig.4-1. From it we can conclude that:

(1) When composition C_0 increasing, the transition range of V/G become smaller.

(2) The beginning transition point of V/G is decreasing, when C_0 increasing. So when C_0 >2wt %, no stable cells can be formed, even velocity as low as V< 1μm/s, at G=3.8 K/mm.

(3) The ending transition point of V/G also decreasing, when C_0 increasing, but it decreasing quicker than the beginning point so make the transition range become narrower.

The critical spacing ($\lambda_{c/d}$), for different compositions, were measured and the results were plotted in Fig. 4-2. The plot of $\lambda_{c/d}(GV)^{1/3}$ vs. V/G shows that, at each constant composition, $\lambda_{c/d}(GV)^{1/3}$ is constant. So $\lambda_{c/d}(GV)^{1/3} \propto f(C_0)$. The value of the constant

was plotted versus composition in Fig. 4-2, to give the critical cell/dendrite transition spacing as:

$$\lambda_{c/d}(GV)^{1/3} = 46.0\ [1/C_0]$$

So $$\lambda_{c/d} = 46.0\ [GV]^{-1/3}[1/C_0]$$

All $\lambda_{c/d}$ data are plotted in Fig. 4-4 to show that all the data collapsed onto a single line which follows the above expression.

Where C_0 is the weight composition (wt %) of the sample. For constant composition sample, at given growth conditions G and V, there will be a spectrum of primary spacing. When cell spacing $\lambda < 46.0\ [GV]^{-1/3}[1/C_0]$, the cell is stable; while when the cellular spacing

$\lambda > 46.0\ [GV]^{-1/3}[1/C_0]$, cell will transform to dendrite.

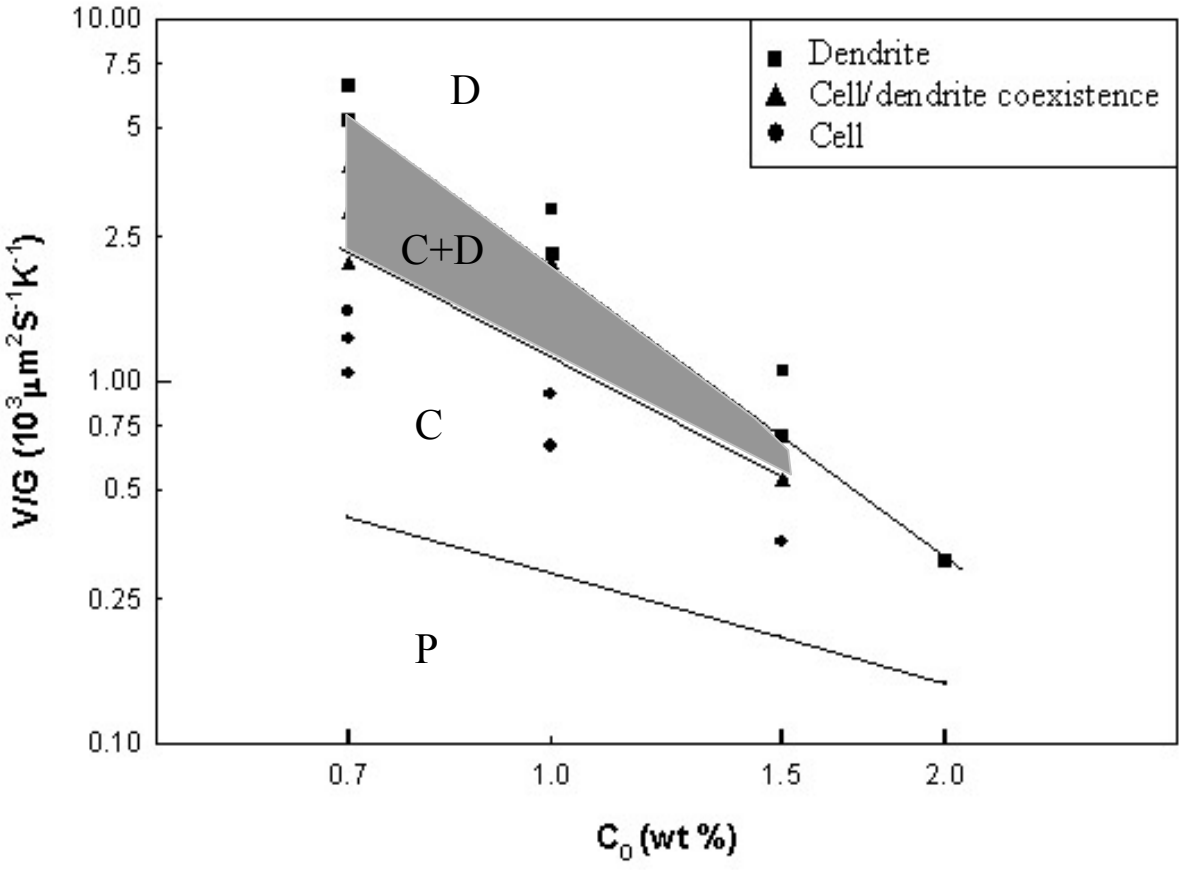

Fig. 4.1 Cell/dendrite transition range of V/G vs. composition.

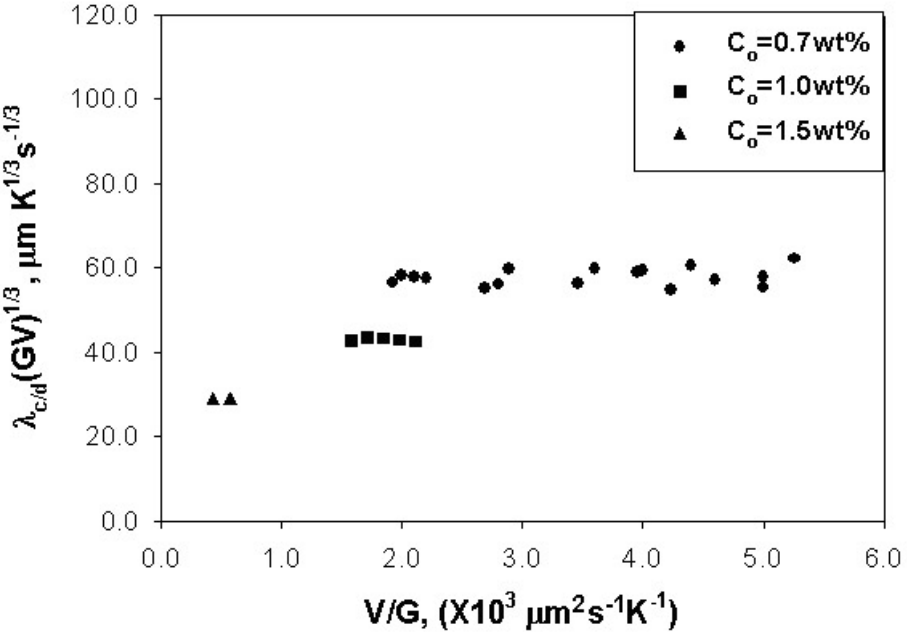

Fig.4-2 Critical cell/dendrite transition spacing and transition condition

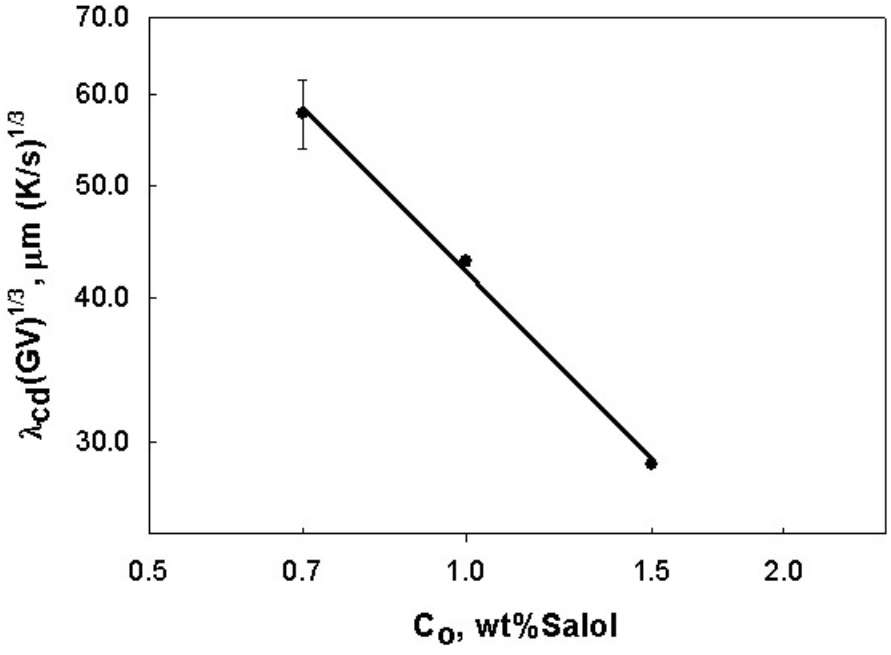

Fig.4-3 Critical spacing for cell/dendrite transition

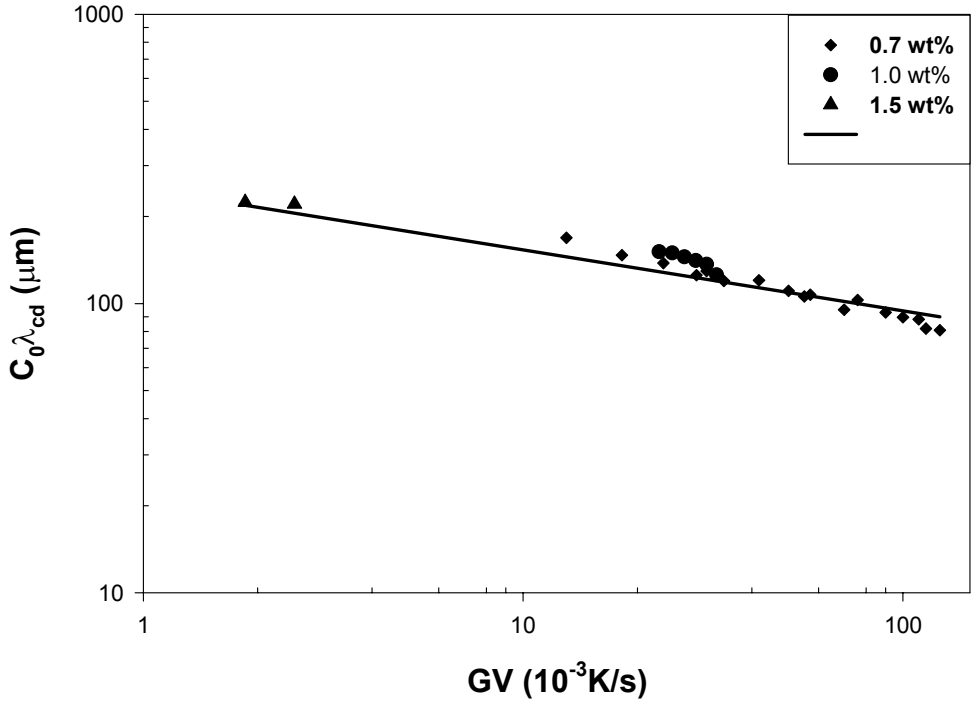

Fig. 4-4 Critical cell/dendrite transition spacing time composition and transition condition for different composition

5. CONCLUSION

Experimental studies in succinonitrile-salol have been carried out to examine the microstructural features of cells. Several new results have been obtained in this study.

1. For a given set of input parameters (G, V, C_0), it is found that multiple solutions of the output parameters are obtained. These output parameters represent microstructural length scales of primary spacing, the length of the mushy zone, cell tip radius and cell width. These microstructural lengths scales have been shown not be independent in that a change of the parameters causes changes in other microstructural scale. In fact, we have established the physical nature of the multiple solutions of primary spacing through experiments and a theoretical model. We have shown that there are four important microstructural lengths that are not independent, but are linked through a definite relationship. This important correlation, given by equation (8), is divided by considering a global balance ahead of a cellular array under steady state growth conditions.
2. The spectrum of primary spacing within an array is shown to influence the cell-dendrite transition condition. Instead of a unique condition, depending on the control parameters, it is shown that the transition occurs over a range of input parameters. A critical condition exit below which cells are stable, and another critical condition above which dendrites are stable. The conditions are experimentally determined, and a region is characterized in which both cells and dendrites coexist. A relationship is developed for the cell/dendrite transition condition that correlates the spacing, thermal gradient, composition and velocity. The critical spacing ($\lambda_{c/d}$), for different compositions, were also measured. At

each constant composition, $\lambda_{c/d}(GV)^{1/3}$ is constant. The numerical calculation shows that the critical cell/dendrite transition is about $\lambda_{c/d} = 46.0\ [GV]^{-1/3}[1/C_0]$, where C_0 is the weight composition of the sample. For constant composition sample, at given growth conditions G and V, there will be a spectrum of primary spacing. When cell spacing $\lambda < 46.0\ [GV]^{-1/3}[1/C_0]$, the cell is stable; while when the cellular spacing $\lambda > 46.0\ [GV]^{-1/3}[1/C_0]$, cell will transit to dendrite.

3. A detail study of the shape of the cell has shown that the cellular shape does not gradually change to parabola when the transition occurs. Rather, a small discontinuity is present in the dimensionless width. When the shape becomes parabolic, sidebranches were found to form, thus, the cell-dendrite criterion based on parabolic tip should be the same as one based on the appearance of sidebranches.

4. The spectrum of spacing that is present under different growth conditions has been characterized, and it is shown that the maximum stable spacing is significantly lower than twice the minimum stable spacing. The ratio of the maximum primary spacing is shown to approach 1.5 for dendritic structures. For cellular arrays, the ratio increasing initially in the cellular regime, reaches a maximum value, and then decreases in the cell-dendrite coexisting region.

6. REFERENCES

1, W. A. Tiller, K A. Jackson, Rutter and B. Chalmers, Acta Metall.

2. M. C. Flemings, Solidification Processing, McGraw Hill (1972).

3. W. Kurz and J. D. Fisher J. D., *Fundamentals of Solidification*, Trans Tech Publ., Aamensdorf, Switzerland, (1995).

4. S. H. Han and R. Trivedi, Acta. Metall. Mater. 42 (1994) p. 25-39.

5. J. Warren and J. S. Langer, Phys. Rev. vol. E47, (1993) p. 2702-2706.

6. J. D. Hunt and S-Z. Lu Metall. Mater. Trans. Vol. 27A (1996) pp.611-623.

7. A. Karma. A. and W-J. Rappel, Phys. Rev. vol. E57, (1998) p. 4323-4326.

8. K. Somboonsuk, J. T. Mason and R. Trivedi, Metall. Trans., vol. 15A (1984) 9 -976.

9. J. D. Hunt In: Solidification and Casting of Metals, Book192, The Metals Society, London. (197p). pp. 3-12.

10. Fisher, Acta Metall. 28:pp.110-202.

11. W. Kurz and J. D. Fisher (1981). Acta Metall. 29:pp.11-20.

12. R. Trivedi, Metall. Trans., vol. 15A (1984) pp.977-984.

13. M. A. Eshelman, V. Seetharaman, and R. Trivedi, Metall. Trans.

14. Akamatsu et al. Acta Metall. 30: pp.21-28.

15. B. Billia, and R. Trivedi, In: *Handbook of Crystal Growth*, edited by D. T. J. Hurle, Elsevier Science Publishers. Vol. 2 (1993) pp. 900-1073.

16. Square root relationship.

17. S. N. Tewari and V. Laxmanan. Metall. Trans. Acta Metall. 31:pp.18-22.

18. Tewari et al. in the Al- Cu system, Bangaloe Symposium

19. J. D. Weeks, W. Van Saarloos and M. Grant, J. Crystal Growth, vol. 112 (1991) pp.244-282.

20. J. D. Weeks and W. Van Saarloos J. Crystal Growth, vol. (199) pp.

21. V. Seetharaman, M. A. Eshelman and R. Trivedi, Metall. Trans. R.

22. R. Trivedi R. and W. Kurz, International Materials Review, vol. 39 (1994). pp.49-74.

23. J. S. Langer, Acta Metall. 19:pp.115-120.

24. A. Karma, Acta Metall. 31:pp.190-205.

25. W. J. Boettinger, S. R. Coriell, A. L. Greer, A. Karma, W. Kurz, M. Rappaz and R. Trivedi, Acta Mater. Vol. 48 (2000) pp. 43-70.

26. K. A. Jackson and J. D. Hunt Acta Metall 33(1965)1061.

27. J. T. Mason and M. A. Eshelman IS-4906, Ames Laboratory, U.S. DOE. Iowa State.

7. ACKNOWLEDGMENTS

To the largest degree I would like to express my sincere gratitude to Dr. Rohit K. Trivedi, my major professor, for his encouragement and accepting me as his student, which provides me the chance to study again in my middle age, to research with direction and to live with open mind.

I would like to thank Dr. R. E. Napolitano for his supporting at the beginning of my graduate study program and giving me the instruction both in the experimental technology and analysis method. I also like to thank Dr. Dennise Vigil for his service on my graduate committee.

I am very grateful to Dr. Shan Liu for sharing research background and ideas and for help during many of the experiments conducted. My appreciation is also extended to all the members in the research group, Mr. Emrah Simsek and Mr. Wenshen He.

I am indebted to my great parents, who have been providing kind care for my dear son during all this long time to support me finish this study. I am also grateful to my lovely son, Zuoming, a healthy and smart boy, who makes me forget all the difficulties in my life.

My special thanks are due to the support and understand from all my kind friends and classmates both in China and in United States.